DEGREE PROJECT, IN SCIENTIFIC COMPUTING , SECOND LEVEL
STOCKHOLM, *SWEDEN 2015*

The role of pairwise and higher-order correlations in feedforward inputs to neural networks

HOW CORRELATIONS IN THE DIVERGENT CONNECTIONS SHAPE EVOKED DYNAMICS

DAVID HÜBNER

KTH ROYAL INSTITUTE OF TECHNOLOGY

SCI SCHOOL OF ENGINEERING SCIENCES

The role of pairwise and higher-order correlations in feedforward inputs to neural networks

How correlations in the divergent connections shape evoked dynamics

D A V I D H Ü B N E R

Master's Thesis in Scientific Computing (30 ECTS credits)
Master Programme in Computer simulation for Science and Engineering (120 credits)
Royal Institute of Technology year 2015
Supervisor at KTH: Arvind Kumar
Examiner was Michael Hanke

TRITA-MAT-E 2015:56
ISRN-KTH/MAT/E--15/56--SE

Royal Institute of Technology
SCI School of Engineering Sciences

KTH SCI
SE-100 44 Stockholm, Sweden

URL: www.kth.se/sci

Abstract

When presented with a task or stimulus, the ongoing activity in the brain is perturbed in order to process the new information of the environment. Typical characteristics of this evoked activity are (1) an increase in firing rate of neurons, (2) a decrease in trial-by-trial variability and (3) an increase or decrease in spike count correlations. Considering the importance of variability and correlations within the rate coding paradigm, it is crucial to understand the origin of these modulations. Different networks in the brain are typically connected through divergent-convergent connections. In a recent work, the correlations in the convergent connections of the feed-forward input have been found to be able to reproduce the above characteristics. This thesis expands this work by also considering correlations in the divergent connections. Through large-scale network simulations, we can show that correlations in the divergent connections have a significant impact on the output correlation coefficient and a small impact on the output firing rate. Moreover, we investigate the question whether keeping the pairwise correlations constant and varying the higher-order correlation structure can influence the network dynamics. We find that this influence is very small suggesting that higher-order correlations in the divergence connections carry only a limited amount of information. These findings can significantly simplify the analysis of neural data.

Rollen av parvisa och högre ordningens korrelationer i indata för framåtkopplade neuronnät

Referat

När hjärnan presenteras med en uppgift eller stimulans, förändras den pågående aktiviteten för att bearbeta den nya informationen om miljön. Typiska egenskaper hos denna förändring av aktivitet är (1) en ökning av spikfrekvens hos nervceller, (2) en minskning i variabilitet mellan försök och (3) en ökning eller minskning av korrelationer räknat i antal spikar. Med tanke på vikten av variabilitet och korrelationer inom ”rate coding” (spikfrekvens-kodning) paradigmet, är det viktigt att förstå ursprunget till dessa aktivitetsförändringar. Olika nätverk i hjärnan är normalt kopplade via divergerande-konvergerande anslutningar. En nylig studie har visat att korrelationerna i ett framåt-kopplat nätverk med konvergerande anslutningar reproducerar de tidigare nämnda egenskaperna hos dessa nätverk. Denna avhandling utökar detta arbete genom att även studera korrelationer i nätverk med divergerande kopplingar. Genom storskaliga nätverkssimuleringar, kan vi visa att divergerande kopplingar har en stor effekt på korrelationskoefficienten men en mindre inverkan på den resulterande spikfrekvensen. Vidare undersöker vi om man kan påverka nätverksdynamiken genom att hålla parvisa korrelationer konstant och variera den högre ordningens korrelationsstruktur. Vi visar att detta inflytande är mycket litet vilket tyder på att högre ordningens korrelationer i divergerade kopplingar endast bär en begränsad mängd information. Dessa resultat kan därigenom avsevärt förenkla analysen av neural data.

Contents

Chapter 1

Introduction

"How is information encoded and decoded in neural networks?" This still unsolved question is one of the most prominent questions in neuroscience. A similar question is: "How do neural networks react to different stimuli in order to encode the new information?" Answering this question would be a crucial step to improve our understanding of neural communication and information processing in the brain.

In this work, a special aspect of this problem is addressed. Namely, how the feedforward input to a neural network can change the dynamics of this network. One could think of the visual system with the pathway from the back of the eye (retina) over a relay center (lateral geniculate nucleus (LGN)) to the visual cortex in the brain. When an animal is presented with a visual stimulus, then the activity in the retina can be significantly perturbed. This perturbation is necessary to process the new information of the environment. Through synaptic connections between different networks in the brain, these modulations can then also affect the downstream activity in LGN and visual cortex.

The underlying idea of this work is that modulating the correlations in the input can reproduce commonly observed dynamics. Positive pairwise correlations, which describe the interaction between the activity of two neurons, are found in almost any part of the brain. Their strength ranges from $+0.02$ in the retina to $+0.25$ in the visual cortex V1 [7]. The main two reasons for the occurrence of correlations are (1) common synaptic input and (2) synchronous activity within a network due to mutual excitation and inhibition [18].

Different networks in the brain are typically connected via convergent-divergent connections. Several previous studies studied the question of how correlations in the convergent connections can affect the networks behaviour. The general findings are that different correlation structures can lead to significantly different firing rates [5, 14], can affect the correlation susceptibility [19, 23] and can reduce the across-trial variability and noise correlations [5]. So, altogether, it is known that the correlational structure in the convergent connections can significantly influence the network dynamics and account for many observed features of the evoked activity.

Despite the interest for modulating the correlation structure in the convergent

connections, fewer research was devoted to the research of the effects of correlations in the divergent connections. Divergent connections are fundamentally different from convergent connections. Correlations in the divergent connections can influence a single neurons behaviour only through network connections. On the other hand, different input statistics in convergent connections directly modulate a single neuron response which in turn can have an effect on the other neurons through synaptic connections. In this work, the main questions is how the correlational structure in the divergent connections can modulate the evoked dynamics. This is linked to the question of how important the precise temporal occurrence of the input spikes is.

While most studies consider pairwise correlation coefficients, fewer studies were done regarding higher-order correlations. Higher-order correlations are a generalization of pairwise correlations for more than two neurons. They describe the strength of interaction for $N = 3, 4, \ldots$ neurons which cannot be yet predicted from the lower-order correlations. It is unclear how important the exact higher-order correlational structure is. In convergent connections, it was shown that keeping the pairwise correlations fixed and changing the higher-order correlations can lead to significantly different dynamics [5, 14].

All these observations lead to two central questions which are investigated in this master thesis:

1. How do correlations in the divergent input connections affect the network dynamics?

2. How important is the higher-order correlational structure in the input distribution?

We want to answer these questions for three network structures which are commonly found in the brain: (1) a neocortex-type of network with mutually and recurrently connected excitatory and inhibitory neurons with distance dependent connectivity, (2) a CA1 (part of the hypothalamus) type network with no recurrent excitation and (3) a purely inhibitory network with no excitatory neurons such as the striatum in the basal ganglia [15].

The details of the neural network models will be introduced in chapter 2. Chapter 3 is then introducing the different input distributions which are used to study the effect of pairwise and higher-order correlations. Chapter 4 is briefly introducing the data analysis methods. The results of the simulations are presented in chapter 5. Finally, the findings are discussed in chapter 6.

1.1 Ongoing Activity

It is known, that the brain is highly active, even in the absence of any specific task. This phenomena is called *Ongoing Activity*. It was shown that the ongoing activity is not just mere noise, but rather reflects all the non-specific inputs and recurrent activities in the brain [1]. Most notably, electroencephalogram (EEG) measurement of the ongoing activity show slow fluctuations over time presumably reflecting varying brain states.

1.2 Evoked Activity

When an animal is presented with a stimuli or task, the ongoing activity is perturbed. This is called the *Evoked Activity*. This activity can be seen as the joint activity of the Ongoing Activity plus all the activity which is related to the new task or stimuli. The key question is how the evoked activity is different from the ongoing activity. A lot of research was devoted to this question and a couple of common features were discovered [6, 17, 21]:

1. The average firing rate of the neurons is increasing
2. The trial-to-trial variability is decreasing
3. Correlations between neurons increase or decrease

See figure 1.1 for an illustration of the first three effects.

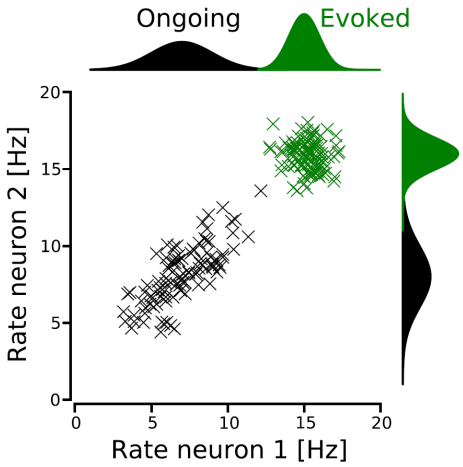

Figure 1.1. Changes from Ongoing to Evoked activity. Each cross is representing the firing rate of a pair of neuron for one trial to the same stimulus. An increase in firing rate (higher mean), a decrease in trial-by-trial variability (lower variance/mean) and a reduction in noise correlation (the firing rates of neuron 1 and 2 become more independent) can be observed. Synthetic data was used.

All these effect are stimulus-induced modulations probably designed to directly encode information or to enhance the encoding and decoding process of information and maximize the usage of the available neural hardware. For instance, a reduction in noise correlations could increase the signal-to-noise ratio of the population rate which would improve a rate-based decoding mechanism [24]. The underlying mechanisms however are only poorly understood. Several mechanism were proposed to explain the evoked activity dynamics. Some of them focus on the network structure to explain the response characteristics. For example, one study attributed these changes to local clusters [16] whereas other studied explained the changed network behaviour by a strict balance between excitation and inhibition [13]. However, these models fail to explain the variation in noise correlations and neglect the importance of the feedforward input statistics in modulating the activity. In a recent approach, it was shown that modulating the input statistics can reproduce most of the observed dynamics [5]. This current work is following the same framework which is based on modifying the two input correlations: within and between correlations. The terms will be explained in the next section.

1.3 Within and Between Correlations

The input to recurrent networks usually arrives via a combination of convergent and divergent connections. Convergent connections describe the case in which many neurons project to a single neuron. In this case, correlated input spikes will sum up and dominate the fluctuations of the membrane potential of the neuron which receives the input. This increases the probability of a spike in the post-synaptic neuron. Thus, convergent connections can directly affect the dynamics of a single neuron which can influence the whole network behaviour through the synaptic connections. On the other hand, divergent projections describe the scenario in which a neuron is projecting to many different neurons which is causing correlations across neurons. Only the temporal summation of these spikes can lead to different effects on single neurons. Hence, divergent connections require network connectivity to have an effect on single neurons.

Because of this fundamental difference, we want to distinguish between two different kinds of correlations in the input statistics: *within* and *between* correlations [5]. The within correlations stem from the convergent connections and refer to the correlations within the presynaptic pool of an individual neuron (input ensemble). The between correlations capture the effect from the divergent projections and refer to the correlation between these input ensembles. See figure 1.2 for an illustration of these terms.

Distinguishing the two different kind of correlations gives us two independent sets of parameters which can be adjusted. However, in realistic scenarios, there are certain limitations to those parameters, because input neurons do not really fall in exactly one of two classes, but rather are a mixture of both. Hence, one kind of correlation is often implying the existence of the other kind of correlation.

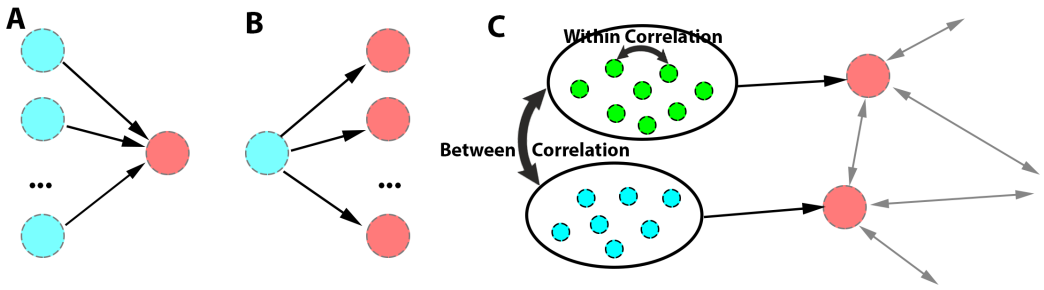

Figure 1.2. Different feedforward projections. **A**: Convergent Connections. **B**: Divergent Connections. **C**: Illustration of within and between correlation in the feedforward input

Another way of seeing it, is in terms of receptive field. A receptive field of a neuron is essentially the area in which a stimulus will trigger the firing of that neuron. Between correlations then correspond to the amount of overlap between the receptive fields.

Several previous studies have researched the effect of modulating the within correlation structure [5, 14, 23] while ignoring the between correlation structure. The general findings are that within correlations determine the spike transmission susceptibility, i.e. how likely it is that an incoming ensemble of spikes is causing a spike in the network. The reason for this effect is that a high within correlation coefficient creates many synchronous input spikes which are significantly depolarizing the neuron resulting in a high chance for a spike.

1.4 Generating Correlated Input Spikes

Different methods were proposed to generate correlated input. They can roughly be divided into two categories [3]: (1) Creating spikes from an inhomogeneous Poisson Processes with a common time-varying rate and (2) generating correlated spike trains by randomly picking spikes from a set of common spike trains, typically a Poisson Process.

Poisson Processes are commonly used because they show similar properties like neural data in terms of the length of interspike-intervals. The underlying *independent-spike hypothesis* assumes that all events are independent of each other. This may violate neural properties such as refractory periods. However, Poisson Processes serve as a good approximation and their simplicity allows for a throughout analytical study.

The key element in the first method is the common time-varying rate. This rate is describing the likelihood of each neuron to fire. All neurons fire then independently of each other, but they have correlated rates due to the common underlying rate. This approach allows to create input with given individual firing rates and

cross-covariance function [3], but does not allow for a direct control of the higher-order cumulants.

The second method is based on the idea of a "mother-process" or "carrier-process". This is usually a Poisson-Process from which spikes are copied into the input spikes trains with either a given probability (Multiple Interaction Process, see [14]) or distribution (Compound Poisson Process, see [27]) . The latter methods allows for choosing different distributions with the same pairwise correlation coefficient, but different higher-order statistics. This gives a great tool to study the effects of changing higher-order statistics and will also be used in this work. The problem is however that the higher-order cumulants cannot be directly controlled.

Both approaches do not allow us to directly control the higher-order rates for $N = 3, 4, \ldots$ neurons. Therefore, we derived another method in this work. The underlying idea is that we directly inject spikes into time bins with predefined individual, pairwise and higher-order firing rates. This has the advantages that we can directly measure the higher-order cumulants of our input distributions. Figure 1.3 shows a comparison of the second and third method. Further details about these two methods will be given in Chapter 3.

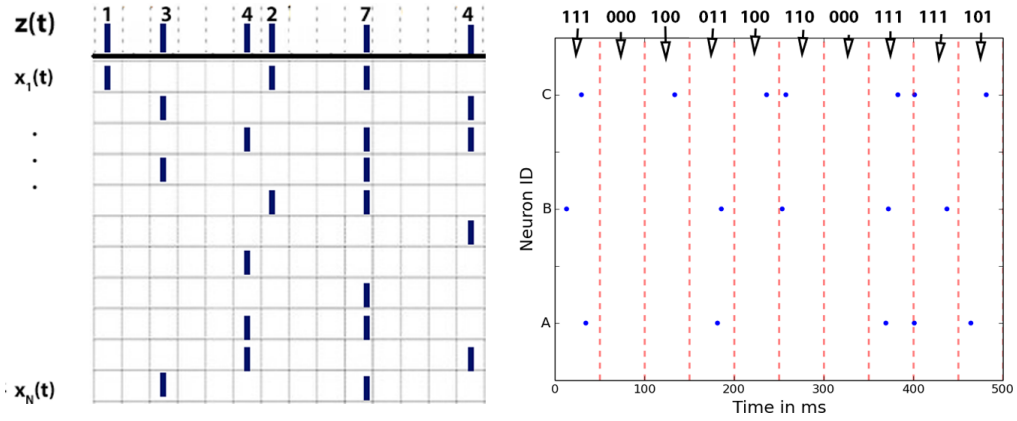

Figure 1.3. Different methods to generate correlated input. Left: Compound Poisson Process. A random number of spikes are randomly copied from the Mother Poisson Process z into the child processes $x_1, ..., x_N$ with the same probability for each child process. **Right**: Spikes are placed in each bin with a predefined probability for each spike pattern.

Chapter 2

Neural Network Model

2.1 Neuron model

To understand neural network dynamics, the single neuron dynamics will be described first. A neuron is a cell with the special property to be electrically excitable. In a single neuron, the difference between the potential inside the cell and outside the cell is normally around -70mV. This is known as resting potential or reversal potential and can vary depending on the concentration of the ions (Na^+, K^+, Cl^-,Ca^{2+}) which are involved. Now, when an impulse from an external source or other neuron arrives at a neuron via a synapse, this potential can increase. This is called depolarization. If the potential exceeds a certain threshold potential (normally around -45 to -55mV), then the neuron fires. This effect is also called *spiking*. It means that in a very short time (few ms), there is first a strong influx of Na^+, depolarizing the cell up to +40mV and then, an outflux of K^+ hyperpolarizing the cell, even below the initial resting potential. This guarantees that the neuron is not firing again for a short time frame called refractory period. Hodgkin and Huxley won a Nobel Prize in 1963 for explaining these dynamics of action potentials. Figure 2.1 (left) shows the shape of an action potential from the Hodgkin and Huxley Model.

2.1.1 Integrate-and-Fire Neurons

In the study of neural networks, it is often not important how the exact shape of the spike looks like. The reason is that we believe that the actual spike shape does not contain much information and can be seen as a unitary event (the neuron is spiking or not). It is only important when the neuron is firing. So in contrast to the full biophysical model, so-called *Integrate-and-Fire* neurons are used. In this model, neurons fire once they reach the threshold potential and the membrane potential is reset to the resting potential. Again, there is a certain time (*refractory period*) in which the neuron cannot fire again. This is mimicked by keeping the membrane potential constant during a time period τ_{ref} after each spike emission. The shape is illustrated in figure 2.1 (right). The obvious advantage is that this model is com-

putationally less expensive and requires less parameters than the Hodgkin-Huxley model, but still provides realistic results.

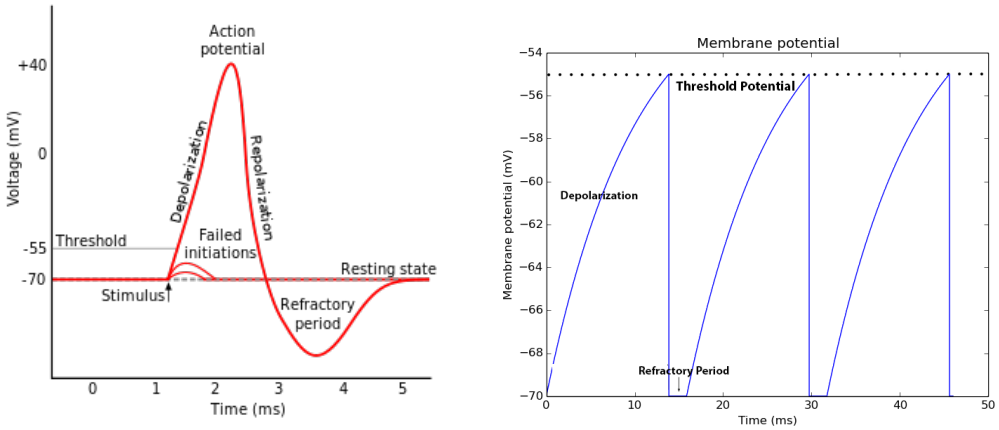

Figure 2.1. Comparison of action potentials. Left: Full shape of an action potential as it can explained with the Hodgkin-Huxley model. Figure adapted from Wikimedia Commons [8]. **Right:** Membrane potential of an integrate-and-fire neuron.

The leaky integrate-and-fire neuron membrane potential is given by the following ordinary differential equation.

$$\frac{dV_m}{dt} = -\frac{1}{\tau_m}(V_m - E_L) + \frac{1}{C_m}(I_E + I_{syn}(t)) \tag{2.1}$$

where the involved quantities are shown in table 2.1.

Symbol	Meaning	Usual Value
V_m	Membrane Potential	
τ_m	Membrane Time Constant	10ms
E_L	Reversal Potential	-70mV
V_{th}	Threshold Potential	-55mV
C_m	Membrane Conductance	200pF
I_E	Constant Current Drive	250pA
τ_{ref}	Refractory Period	2ms
I_{syn}	Synaptic Inputs	

Table 2.1. Neuron Parameters

This equation (2.1) describes the temporal change in membrane potential as depending on two factors: (1) On the tonic inputs I_E and synaptic inputs I_{syn} with efficiency $\frac{1}{C_m}$ and (2) on a leak term reflecting the diffusion of ions that occurs through the membrane when some equilibrium is not maintained in the cell.

This causes the membrane potential to return to the resting potential if no further synaptic input is received.

2.2 Synapse Model

Neurons are connected by synapses. These are direct connections which transfer a pulse from a presynaptic neuron to a postsynaptic neuron. Depending on the type of neuron (excitatory / inhibitory), this pulse can either increase or decrease the postsynaptic membrane potential, respectively. In the simulations in this work, alpha-shaped synapses are used. More precisely, for a given spike at time $t_i^{(f)}$, the influence on the postsynaptic neuron is given by $J_{ij}\alpha(t - t_i^{(f)})$ where the synaptic weight J_{ij} is a measure of the efficacy of the synapse from neuron i to neuron j and $\alpha(t)$ is the synaptic link function given by:

$$\alpha(t) = \frac{t}{\tau_s} \cdot \exp\left(1 - \frac{t}{\tau_s}\right) \tag{2.2}$$

where $\tau_s = 2ms$ is the synaptic time constant. The shape of the postsynaptic strength for $J = 1$ is shown in figure 2.2. It shows that the largest input arrives after 2ms and a substantial amount of input arrives for around 10ms.

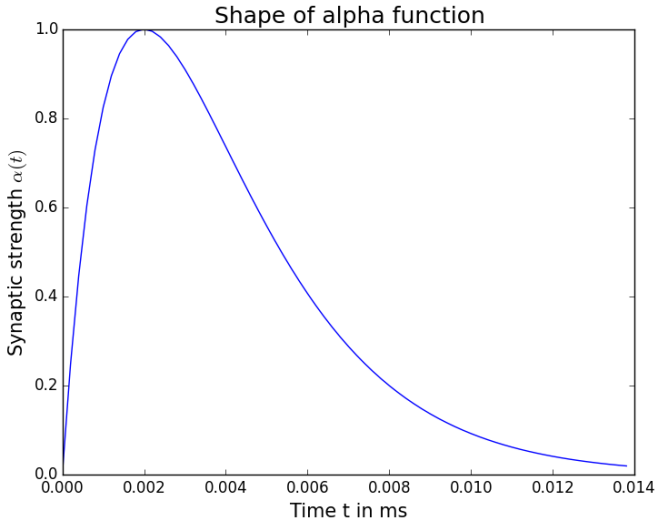

Figure 2.2. Synaptic link function

The synaptic current strength from all inputs is then given by

$$I_{syn}(t) = \sum_j J_{ij} \sum_f \alpha(t - t_i^{(f)}) \tag{2.3}$$

Table 2.2 shows an overview of all synapse parameters.

Symbol	Meaning	Usual Value
τ_s	Synaptic Time Constant	2ms
J_{exc}	Excitatory Synaptic Strength	varies, see appendix
g	E/I Ratio $J_{inh} = -g \cdot J_{exc}$	5
d	Synaptic Delay	2ms

Table 2.2. Synapse Parameters

The resulting neuron/synapse model has 5 parameters for the neuron model $(\tau_m, E_L, V_{th}, C_m, I_E)$ and 2 more parameters for the synapse (τ_s, J_{ij}) resulting in a total number of 7 parameter assuming that the synaptic strengths are constant.

2.3 Network Model

Different network architectures and connectivity profiles will be studied in this work. Typical model consider networks of excitatory(E) and inhibitory(I) neurons in which both the populations are mutually and recurrently connected. The ratio of excitatory to inhibitory neurons is usually about 4 to 1. These networks corresponds to a class of networks similar to the neocortex. Other brain regions however exhibit connectivity which is devoid of excitatory to excitatory connections (e.g. the CA1 region of the hippocampus and the medial entorhinal cortex) or excitatory neurons are altogether absent (e.g. striatum, central nucleus of the amygdala, globules pallidus) [15].

Small-world networks are networks in which each node can be reached from every other node by a small number of connections. Examples can be found in many fields, e.g. in social networks or electric power grids. It was found that many neural networks also possess the small-world property. One example is the worm C. elegans which was the only organism to have its connectome (neuronal "wiring diagram") completed [30]. This complete map of all 302 neurons with their 7,000 connections also showed the small-world property. A popular way to generate small-world networks is the Watts-Strogatz model [29]. It allows to continuously move from a completely random network to a very structured network. In our network simulations, we choose 80% of the connections from within 20% of the closest neurons and the other 20% of the connections from the remaining 80% of the neurons. An illustration of the three different networks can be seen in figure 2.3.

Typically, we simulate a network with 5000 neurons. The connection probability is 10% which results in a relatively sparsely connected network. From those 5000 neurons, 1000 neurons receive correlated input. Additionally to the tonic drive I_E, the neurons may receive external independent Poissonian input with frequency ν_{ext} and synaptic strength J_{ext}. Table 2.3 summarizes all network parameters.

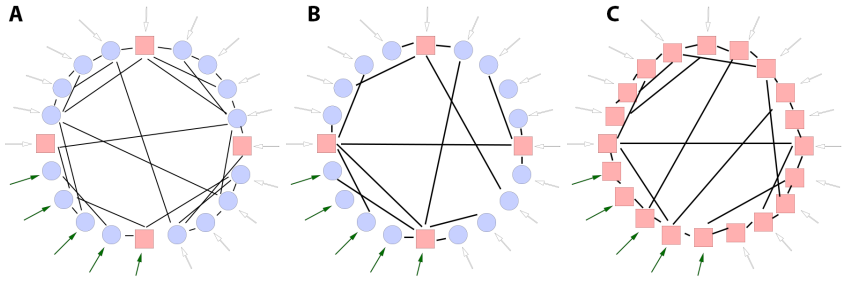

Figure 2.3. Different connectivity profiles. Blue circles represent excitatory neurons, red squares represent inhibitory neurons. Each neuron gets some independent external drive (marked by blank arrows) and one part of the network gets correlated input (green arrows). The connecting probability is distance-dependent (see text). **A:** Randomly connected ring network with both recurrently and mutually connected excitatory and inhibitory neurons. **B:** Network devoid of E to E connections. **C:** Purely inhibitory network.

Symbol	Meaning	Value
N	Number of neurons	5000
P_{rew}	Renewal probability for small-world network. Determines percentage of short distance connections.	20%
N_{Stim}	Number of stimulated neurons	1000
ϵ	Connecting probability	10%
	Ratio of excitatory to inhibitory neurons	4:1
ν_{ext}	External Poisson rate	varies, see appendix
J_{ext}	External synaptic strength	varies, see appendix

Table 2.3. Network Parameters

2.4 Computer Simulations in NEST

To conduct large-scale neural network simulations, a NEural Simulation Tool (NEST) was developed. The software was developed in 2004 and is most suited to simulate the dynamic and structure of large neural networks rather than detailed morphological properties of single neurons [11]. The kernel of NEST is written in C++ guaranteeing a very good performance. It comes with a native simulation language interpreter called SLI. An attractive alternative is a Python user interface called PyNEST [10]. Python is free, it has a more convenient syntax and gives access to many supplementary packages, like the Matplotlib/Pylab library to visualize the data directly from within the simulation script or the Numpy or NeuroTools package to analyze the data.

NEST uses advanced techniques to minimize numerical errors. For a large class of neuron models, e.g. the integrate-and-fire neurons, NEST integrates the dynamic equations with machine precision by using a technique termed *Exact Integration* in the context of pulse coupled neuronal systems [20]. Integrate-and-fire neurons can be seen as a series of a dynamic linear part (sub-threshold leaky integration of inputs) and a static non-linearity (the threshold operation). The integration method in NEST uses the matrix exponential to exactly integrate systems with this kind of simple non-linearity. The time steps for the simulations were chosen to be 0.1ms.

Chapter 3

Input Distributions

In this chapter, two approaches are presented to generate the input. The first approach is a Compound Poisson Process which allows us to generate input with a predefined individual and pairwise correlation coefficient, but without direct quantification of the higher-order correlations. The second approach, a bin-wise insertion of spikes, will allow us to also control the higher-order correlations. Before presenting these approaches, a brief introduction to higher-order correlations is given.

3.1 Higher-Order Correlations

3.1.1 Pairwise Correlations (N=2)

To understand higher-order correlations, it is useful to look at the case of $N = 2$ first. The covariance between two real valued random variables S_1 and S_2 is then defined as:

$$Cov(S_1, S_2) := E[S_1 - E[S_1]]E[S_2 - E[S_2]] \tag{3.1}$$

which is a common measure for the degree of dependence between the two random variables. This quantity can be normalized to obtain the well-known Pearson's Correlation Coefficient

$$c = \frac{Cov(S_1, S_2)}{\sqrt{Var[S_1][Var[S_2]}}. \tag{3.2}$$

By using the linearity property of expectations, one can rewrite the covariance as

$$Cov(S_1, S_2) = E[S_1 S_2] - E[S_1]E[S_2]. \tag{3.3}$$

Thinking of spike trains, the S_i are binary values which indicate a spike/ no spike within a certain time window. Then the expectation $E[S_i]$ equals the probability

p_i of a spike. Similarly, $E[S_1S_2]$ is the probability that both neurons spike within the same time bin. This implies that the covariance is subtracting the probability of a coincidence by chance from the actual probability of two synchronous spikes. If the neurons would be independent of each other, then the covariance equals 0. A correlation coefficient of 1 would indicate that both neurons are perfectly synchronous, a correlation coefficient of -1 would indicate that both neuron perfectly inhibit each other.

3.1.2 Higher-Order Cumulants (N>2)

The natural generalization of the pairwise covariance is given by the connected cumulants. The idea is to quantify the dependence of the tuple $(S_1, S_2, ..., S_N)$ that is not already contained in the $(N-1)$th order cumulant. In the case of $N = 3$, the third-order cumulant which measure the dependency of (S_1, S_2, S_3) which is not yet contained in the pairwise correlations.

A naive approach would be to subtract the probability that N neurons spike together by chance from the probability of those N spiking together assuming that they are independent of each other. In the case of $N = 3$ this would read as

$$E[S_1S_2S_3] - E[S_1]E[S_2]E[S_3]. \tag{3.4}$$

This term would disappear if all three neurons are independent of each other. However, there are some partial dependencies which also have to be considered. Assuming a correlation between S_1 and S_2, but both are independent of S_3, we have that

$$E[S_1S_2S_3] \overbrace{=}^{independent} E[S_1S_2]E[S_3] \overbrace{\neq}^{(S_1,S_2)\text{ correlated}} E[S_1]E[S_2]E[S_3] \tag{3.5}$$

Even though the dependence in this scenario is only pairwise, the term in equation (3.4) would not disappear. This violates the statement that the third-order cumulant measures the degree of dependence which is not yet contained in the second-order cumulants. To correct for this, we have to subtract the pairwise dependencies as well. In this case, the pairwise cumulants (covariances) occur in the form of $Cov(S_i, S_j)E[S_k]$ for $i, j, k = 1, 2, 3$ pairwise different. Putting everything together, the third-order cumulant reads as:

$$\begin{aligned} k_3 = {} & E[S_1S_2S_3] - E[S_1]E[S_2]E[S_3] - Cov(S_1, S_2)E[S_3] \\ & - Cov(S_1, S_3)E[S_2] - Cov(S_2, S_3)E[S_1] \end{aligned} \tag{3.6}$$

Using the covariance formula from before in equation (3.3), this can be rewritten as:

$$\begin{aligned} k_3 = {} & E[S_1S_2S_3] + 2E[S_1]E[S_2]E[S_3] \\ & - E[S_1S_2]E[S_3] - E[S_1S_3]E[S_2] - E[S_2S_3]E[S_1]. \end{aligned} \tag{3.7}$$

Cumulants play an important role in statistics where they often occur as sums of the raw moments $\mu_k(S) = E[S^k]$. To derive the formulas of the higher-order cumulants, one has to know the relationship between the moment-generating function $M(t)$ and the cumulant generating function $g(t)$, namely:

$$M(t) = 1 + \sum_{n=1}^{\infty} \frac{\mu_n t^n}{n!} = \exp\left(\sum_{n=1}^{\infty} \frac{\kappa_n t^n}{n!}\right) = \exp(g(t)). \tag{3.8}$$

Thus, the cumulant-generating function is the natural logarithm of the moment-generating function. The cumulants can then be recovered in terms of moments by evaluating the n-th derivative of $\log M(t)$ at $t = 0$:

$$\kappa_n = g^{(n)}(0) = \frac{\mathrm{d}^n \log M(t)}{\mathrm{d}t^n}\Big|_{t=0}. \tag{3.9}$$

To find the explicit expressions for the n-th order cumulants in dependence of the n-th moments, one can use the Faà di Bruno's formula for higher derivatives of composite functions which lead to the expression

$$\kappa_n = \sum_{k=1}^{n} (-1)^{k-1}(k-1)! B_{n,k}(\mu_1, \ldots, \mu_{n-k+1}) \tag{3.10}$$

where $B_{n,k}$ are partial Bell polynomials.

The formulas for higher-order cumulants gets increasingly more difficult for higher N. In contrast to the pairwise correlation coefficient, it is not possible to normalize the higher-order cumulants which makes it difficult to directly interpret the values of the cumulants. In this work, the terms higher-order cumulants and higher-order correlations will mean the same. A more throughout introduction to higher-order correlations is given in [26].

3.2 Compound Poisson Process

This approach to generate input is based on a "carrier-process" $z(t)$ from which spikes are copied into the input spikes trains $x_1(t), \ldots, x_N(t)$ with a given amplitude distribution $f(k)$ [27]. The "carrier process" is a Poisson Process which means that the waiting time between two events is distributed as an Exponential Distribution with rate λ, i.e. the probability density function of the waiting times is given by:

$$p(x;\lambda) = \begin{cases} \lambda e^{-\lambda x} & x \geq 0, \\ 0 & x < 0. \end{cases} \tag{3.11}$$

Let the amplitude A now be a random variable defined on the discrete domain $\{1, \ldots, N\}$ with probability mass function (pmf) $f(k)$. Whenever there is a spike

in the carrier process, a random number r from the amplitude distribution $f(k)$ is drawn. The spike of the carrier process is then randomly copied into r of the child trains $x_1(t), \ldots, x_N(t)$. So amongst all N child trains, a subset of r trains is picked and a spike is inserted in each of these trains. Each subset has the same probability to be picked. An illustration of a Compound Poisson Process is shown in figure 3.1.

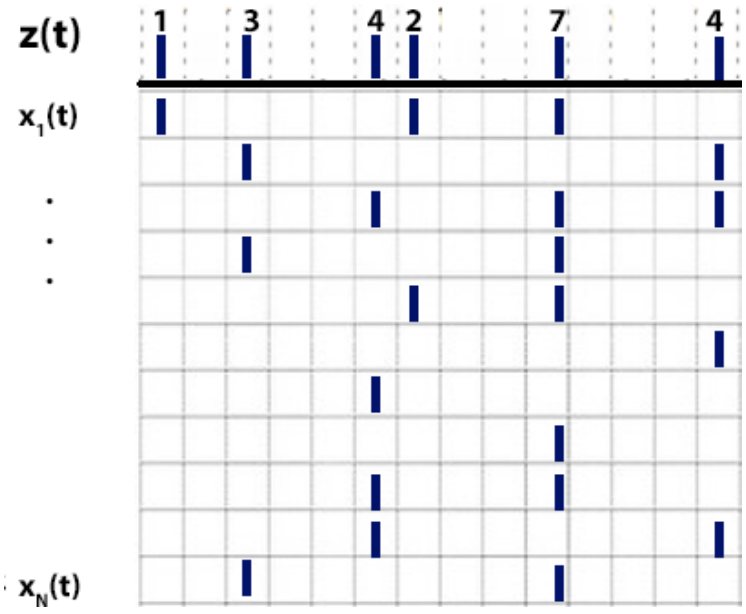

Figure 3.1. Compound Poisson Process. z(t) is a Poisson Process from which spikes are randomly copied into a number of child trains $x_1, \ldots, x_N(t)$. The number of copies r is drawn from the amplitude distribution f(k) and written above the spike of the mother train.

One important result from literature is that the pairwise correlation coefficient of a Compound Poisson Process can directly be calculated from the amplitude distribution and is independent of the rate of the carrier process [27]. It is given by:

$$\rho = \frac{\frac{E[A^2]}{E[A]} - 1}{N - 1} \tag{3.12}$$

3.2.1 Different Amplitude Distributions

Based on the Compound Poisson Process, we can now construct different amplitude distribution which lead to the same pairwise correlation coefficient. The following three distributions will be used:

1. A log series distribution with pmf $f(k) = \frac{p^k}{k \cdot log(1-p)}$,

2. a geometric distribution with pmf $f(k) = (1-p)^{k-1} \cdot p$ and
3. a binomial distribution with pmf $f(k) = \binom{N}{k} p^k (1-p)^{N-k}$.

In all cases, the free parameter p was fitted to match a predefined pairwise correlation coefficient with equation (3.12). The distribution were also rescaled to have mass 1 on $\{1, \ldots, N\}$ by taking $\frac{f(k)}{\sum_{k=1}^{N} f(k)}$ as pmf. Figure 3.2 shows the three different amplitude distributions for $N = 1000$ and $\rho = 0.15$.

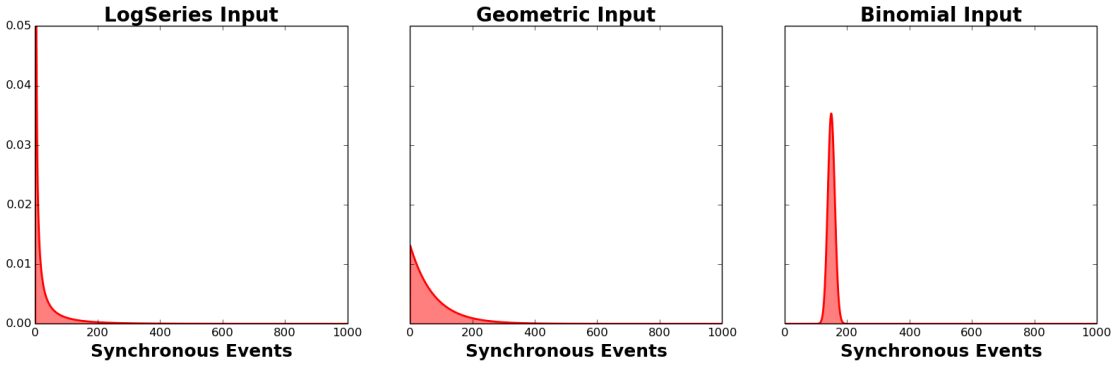

Figure 3.2. Different Amplitude Distriubtions

Additionally to the pairwise correlation coefficient, we also want to control for the firing rates. Therefore, the rate of the carrier process has to be adjusted in dependence of the expected value of the amplitude distributions. Assuming that we want an input with a frequency of f_S per neuron, we can then calculate the rate f_C of the carrier process as

$$f_C = \frac{f_S \cdot N}{E[A]} \tag{3.13}$$

With this approach, we derived input distributions with the same firing rates and pairwise correlation coefficients, but a different higher-order correlation structure. However, the downside of this approach is that we do not have direct control over the higher-order correlations, i.e. we cannot quantify them directly.

3.3 Bin-wise Data Generation

To overcome the weaknesses of the Compound Process that we cannot directly measure the higher-order correlation, we developed an alternative approach. The idea is to directly insert spikes into small time bins so that we can specify individual, pairwise, triple-wise and higher-order interactions. To give an example, we can think

of a scenario with $N = 3$ neurons. There, we have $2^3 = 8$ different possible spiking patterns $(0, 0, 0), (1, 0, 0), ...(1, 1, 1)$ where the 1 denotes a spike and the 0 denotes silence. Figure 3.3 shows a visualization.

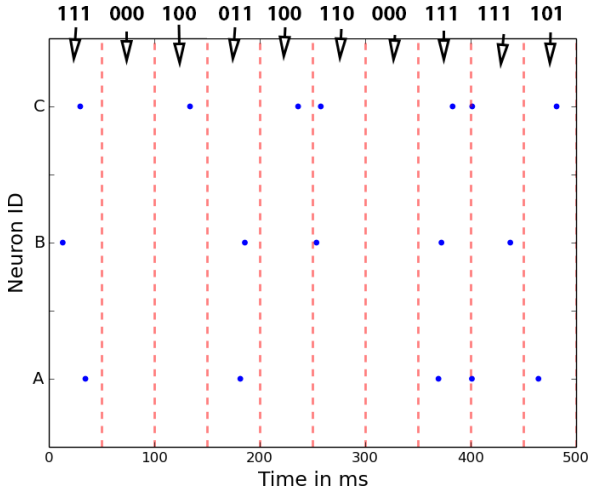

Figure 3.3. bin-wise approach to generate data.

If we now specify the probabilities for all of these 8 possible patterns, we can sample from this distribution by moving from bin to bin and sample from the pattern distribution. This will give us an input distribution where we have direct control of all orders of interactions and thus, we can analytically calculate the higher-order cumulants and other quantities like the entropy of the input.

3.4 Zero Higher-Order-Correlations

The goal of this section is to generate spike trains with given individual firing rate μ and pairwise correlation coefficient c, but with zero higher-order cumulants. This can be useful to isolate the effects of higher-order correlations and to create a distribution which is very different from other distributions. The necessary equations will be derived and solved combinatorially. Finally, an algorithm will be presented to compute the probabilities and the limitations of this method are discussed.

3.4.1 A Distribution with Zero Higher-Order Correlations

In the following, it should be assumed that all neurons have the same firing rate $E[S_1] = E[S_2] = ... = E[S_N]$, the same pairwise correlation coefficients, the same triple-wise cumulants and so forth. This means that we want to assume that all neurons have the same statistical properties. Because we see neurons as binary (spiking / not-spiking), we want to think in terms of probabilities instead of ex-

pectations. The following notation is then used for the probability of synchronous spikes without taking into account whether the other neurons are spiking or not:

$$p_1 := E[S_1] \tag{3.14}$$
$$p_{11} := E[S_1 S_2] \tag{3.15}$$
$$p_{111} := E[S_1 S_2 S_3] \tag{3.16}$$
$$... \tag{3.17}$$

Note that $p_1 = \mu$ is the firing rate.

Using this notation, we can then compute the pairwise firing rate p_{11} in dependence of the individual firing rate and the pairwise correlation coefficient c. The formula for the pairwise correlation coefficient (equation (3.2)) reads with the new notation as:

$$c = \frac{p_{11} - p_1^2}{p_1(1-p_1)} \iff p_{11} = cp_1(1-p_1) + p_1^2 \tag{3.18}$$

In the scenario of a homogeneous population, the connected cumulants now read as:

$$\kappa_1 = p_1 \tag{3.19}$$
$$\kappa_2 = p_{11} - p_1^2 \tag{3.20}$$
$$\kappa_3 = p_{111} - 3p_{11}p_1 + 2p_1^3 \tag{3.21}$$
$$\kappa_4 = p_{1111} - 4p_{111}p_1 - 3p_1^2 + 12p_{11}p_1^2 - 6p_1^4 \tag{3.22}$$
$$... \tag{3.23}$$

To derive the zero higher-order correlation distribution, we require that the first two cumulants should be kept constant while the higher-order cumulants should be all zero:

$$\kappa_3 = \kappa_4 = ... = 0 \tag{3.24}$$

This results in a non-linear system with $N-2$ equations and $N-2$ unknowns (the probabilities p_{111}, p_{1111}, etc). Because it is a non-linear system, the general solution is difficult to obtain by numerical approximation. An analytical solution can be found by using a combinatorial approach.

3.4.2 Combinatorial Solution

The solution is using the fact that the moments can be expressed in terms of cumulants via the following equation:

$$E(S_1 \cdots S_n) = \sum_{\pi} \prod_{B \in \pi} \kappa(S_i : i \in B) \tag{3.25}$$

where π runs through the list of all partitions of $\{1, \ldots, n\}$ and B runs through the list of all blocks of the partition π. For example for $N = 3$, we get:

$$\begin{aligned} E(XYZ) =& \kappa(X,Y,Z) + \kappa(X,Y)\kappa(Z) + \\ & \kappa(X,Z)\kappa(Y) + \kappa(Y,Z)\kappa(X) + \kappa(X)\kappa(Y)\kappa(Z) \end{aligned} \tag{3.26}$$

Now, we require that all higher-order cumulants ($N > 2$) are zero, e.g. $\kappa(X,Y,Z) = 0$. This means that we end up only with those partitions where all blocks have size two or less. Let us denote the cumulants of blocks with two elements as $\kappa_2 = \kappa(X,Y) = ...$ and the cumulants of blocks with one element as $\kappa_1 = \kappa(X) = ...$

The combinatorial task is now to determine the exact number of those blocks. First, the complete formula is given and then it will be explained. The probability of n neurons spiking together is given by:

$$p_{\underbrace{11\ldots1}_{n}} = \sum_{j=0}^{\lfloor \frac{n}{2} \rfloor} \frac{\frac{n!}{2^j}}{j!(n-2j)!} \kappa_2^j \kappa_1^{n-2j} \tag{3.27}$$

The formula can directly be derived from equation (3.25). The sum is taken over all possible partitions with all blocks sizes less and equal two. Here, j is counting the number of blocks with size 2 whereas $(n-2j)$ is counting the number of blocks with size 1. To get the number of possible partitions for a given j, the multinomial coefficient has to be used:

$$\binom{n}{j \quad (n-2j)} = \frac{n!}{j!(n-2j)!} \tag{3.28}$$

This gives the number of possible arrangements of dividing n elements into j blocks of size 2 and $(n-2j)$ blocks of length 1. In this case however, blocks with identical elements, but different order are counted twice (e.g. $\kappa(X_1, X_2)$ and $\kappa(X_2, X_1)$). Therefore, we have to correct for all possible permutations in the blocks. Each block of size 2 has two possible permutation, thus we have to divide this multinomial coefficient by 2^j to get the final equation (3.27).

3.4.3 Computing the Pattern Probabilities

So far, we calculated the individual rates p_1, pairwise rates p_{11}, etc. which create zero higher-order cumulants ($N > 2$). The last step is to compute the complete pattern distribution. In the scenario of $N = 3$, we are interested in computing the following 8 probabilities $p_{000}, p_{001}, p_{010}, p_{011}, p_{100}, p_{101}, p_{110}$ and p_{111}. Because we

assumed homogeneity, this reduces to

$$D_0 = p_{000} \tag{3.29}$$
$$D_1 = p_{100} = p_{010} = p_{001} \tag{3.30}$$
$$D_2 = p_{110} = p_{101} = p_{011} \tag{3.31}$$
$$D_3 = p_{111} \tag{3.32}$$

where D_k denotes the probability of exactly k spikes. First, we note that $D_3 = p_{111}$ and that there are $\binom{N}{k}$ patterns with exactly k spikes. Now, we can go backwards to obtain the other three probabilities D_0, D_1 and D_2.

From $p_{11} = p_{111} + p_{110}$, we get that $D_2 = p_{110} = D_3 - p_{11}$.

From $p_1 = p_{100} + p_{110} + p_{101} + p_{111}$, we get that $D_1 = p_{100} = p_1 - 2 \cdot D_2 - D_3$

Because all the probabilities have to sum to 1, we get that $D_0 = 1 - 3 \cdot D_1 - 3 \cdot D_2 - D_3$ which gives us all desired pattern probabilities.

This procedure can be generalized for the case of $N > 3$ which results in the following algorithm:

3.4.4 Pseudo-Code Algorithm

Input : N - Number of Neurons
μ - Firing Rate
c - Pairwise Correlation Coefficient
Output: $D_0, D_1, ..., D_N$ - Probabilities of exactly 0,1,...N spikes

Algorithm: Compute variance $\sigma^2 = c \cdot (1 - \mu)\mu$
for *n=0:N* **do**
  Calculate $\mu_n = \sum_{j=0}^{\lfloor \frac{n}{2} \rfloor} \frac{\frac{n!}{2^j}}{j!(n-2j)!} \sigma^{2j} \mu^{n-2j}$
end
for *k=0:N* **do**
  Compute $D_{N-k} = \mu_{N-k} - \sum_0^{k-1} \binom{k}{l} \cdot D_{N-l}$
end
return $D_0, D_1, ..., D_N$

Algorithm 1: Generating a distribution with zero higher-order cumulants

3.4.5 Limitations

In this algorithm, the probabilities of spikes are calculated. Those probabilities can only take values in $[0, 1]$. Hence, the algorithm has a limited choice of feasible combinations of N, μ and c. A general rule of thumb is that the inequality $c \leq \frac{1}{N}$ should be satisfied to get a valid solution of this system. If we choose this bin-wise approach to generate data, we will take $N = 50$ and $c = 0.02$.

3.5 Maximum Entropy Models

In this section, the idea of maximum entropy models is introduced. First, a general introduction to maximum entropy models is given. It is inspired by [32]. Then an application as in [22] is given. Finally, a maximum entropy distribution for a homogeneous population with fixed individual and pairwise firing rates is derived as in [2].

3.5.1 Introduction

The idea of maximum entropy models is best explained with an example. Imagine that the data from $N = 3$ neurons was recorded. Only the spiking times were measured. The data was then binned into bins with a predefined length of 20ms. For each bin, it is observed whether a neuron is spiking (1) or not (0) (see section 3.5.1). Ideally, the bin size is chosen so small that there will be at most one spike per bin. In the rare case of two spikes per bin, this bin will still be denoted with (1).

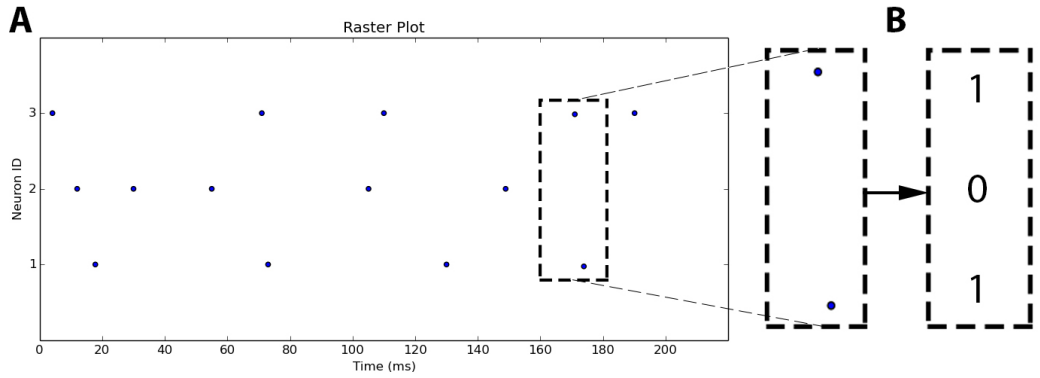

Figure 3.4. Binning example with bin width 20ms. **A**: Raster Plot: Each dots represents one spike of a given neuron at a given time. **B**: Vector representation for one time bin: For each bin 1 corresponds to a spike, 0 corresponds to no spike.

Based on this representation, the activity of the neuron with ID 1 in the above figure with a bin size of 20ms bins would read as $\sigma_1 = (1, 0, 0, 1, 0, 0, 1, 0, 1, 0)$ representing the binning of the spiking times (18ms,72ms,132ms,174ms). The average firing rate of neuron i is then given by:

$$< \sigma_i >= \frac{1}{T} \sum_{t=1}^{T} \sigma_i^t \tag{3.33}$$

where T is the total number of time bins, the angled bracket denotes the time average and the superscript t represents the bin number. Similarly, the pairwise rates are given by:

$$< \sigma_i \sigma_j >= \frac{1}{T} \sum_{t=1}^{T} \sigma_i^t \sigma_j^t \tag{3.34}$$

The state vector at a given time bin t, V^t, then represents the states of the neuron (out of 2^N states) at a particular time bin and is defined as:

$$V^t = \begin{bmatrix} \sigma_1^t \\ \sigma_2^t \\ \sigma_3^t \end{bmatrix} \tag{3.35}$$

Now, imagine that we want to fit a model which has the same individual and pairwise rates as the neurons observed in our recordings. The output of the model will be the probability of all 2^N patterns: (000,001,011,...). To simplify the analysis, we assume stationary, i.e. the pattern probability does not change over time. Since we have three neurons, fixing the individual rates gives three equations. For the pairwise rates, there are again three possible pairs, giving us another three equations. One more equation comes from the fact that all pattern probabilities have to sum up to 1. This gives us $1 + 3 + 3 = 7$ equations for $2^3 = 8$ unknowns. Thus, we have an under-determined system and an infinite number of models that can fit the given constraints. To obtain an unique solution, we will use the maximum entropy approach. Remember, that the entropy is defined as [32]

$$S = -\sum_{i=1}^{2^N} log(P(V_i)) \cdot P(V_i) \tag{3.36}$$

and is a measurement for the uncertainty or amount of information in a system. Amongst all possible models which fit the data, we will now choose that model with the highest uncertainty or highest entropy. Another way of phrasing it, is to say that we pick the model that fits the data and makes the least assumptions about the third-order interactions. This gives us now one more constraint and makes it possible to obtain a unique solution of the system.

3.5.2 Application

Maximum entropy models were used to successfully fit data recorded from a salamander retina [22]. The data had relatively low firing rates 0.4-4.5Hz and weak pairwise correlation coefficient (mean around 0.02, estimated from Figure 1D in that paper). The fitting was done in two steps. First, a first-order maximum entropy model only replicating the individual firing rates was computed. From this model, the entropy S_1 was measured and compared with the entropy of the data S, i.e. $I_N := |S_1 - S|$ was computed. I_N is a "measurement of the total amount of correlation in the network, independent of whether it arises from pairwise, triplet or

more-complex correlations". It was found that I_N is relatively large which suggests that the first order model is not suited to fit the data, even though the pairwise correlations are weak.

The second step is then to fit a second-order maximum entropy model by also replicating the pairwise rates and again measuring the entropy S_2 of that fit. The success of the second-order maximum entropy models in capturing the correlation structure of the network is then summarised by the fraction $\frac{I_2}{I_N}$ which is around 90% independent of many details. It was also shown that fitting a second-order maximum entropy model in the cortex can also explain 88% of the correlational structure [28]. These findings suggest that individual and pairwise firing rates are sufficient to describe the pattern distributions and the higher-order correlation structure plays a less significant role. However, it was shown that changing the higher-order correlations while keeping the individual firing rates and pairwise correlation constant in the within correlations can have a significant impact [5], e.g. it can lead to firing rate differences of more than 100%. The impact on between correlations is however not well studied yet.

3.5.3 Derivation of a Maximum Entropy Distribution

In this subsection, a maximum entropy distribution for given individual firing rate μ and pairwise correlation coefficient c is given as in [2] . The main assumption is that all neurons are statistically indistinguishable, i.e. have the same properties. This means that all individual rates $< \sigma_i >$, pairwise rates $< \sigma_i \sigma_j >$ and higher-order rates are the same. Based on this central assumptions, the probability space reduces to $N+1$ unknowns $D_0, D_1, ..., D_N$ which describe the occurrence of $0, 1, ..., N$ spikes at the same time as introduced before.

For each $k \in \{0, \ldots, N\}$, there are $\binom{N}{k}$ different pattern with exactly k spikes. For instance for $N = 4$ and $k = 2$, there are the possibilities 1100, 1010, 1001, 0110, 0101, 0011 to exactly generate 2 spikes with 4 neurons. Because the probabilities have to sum up to 1, we obtain the first condition

$$1 = \sum_{k=0}^{N} \binom{N}{k} D_k. \tag{3.37}$$

To obtain the firing probability of one specific neuron, we have to take all pattern into account where this specific neuron is firing:

$$p_1 = \sum_{k=1}^{N} \binom{N-1}{k-1} D_k. \tag{3.38}$$

Similarly, the probability that any two neurons fire is given by:

$$p_{11} = \sum_{k=2}^{N} \binom{N-2}{k-2} D_k. \tag{3.39}$$

We can again relate the pairwise correlation coefficient c and the pairwise firing rate with equation (3.18) $p_{11} = cp_1(1-p_1) + p_1^2$ from before. To obtain the other equations, we will maximize the entropy. The entropy in terms of pattern probability is given by:

$$S = -\sum_{k=0}^{N} \binom{N}{k} D_k ln(D_k). \tag{3.40}$$

Maximizing is then done by setting the partial derivatives to zero.

$$\frac{\partial S}{\partial D_k} = 0 \quad \text{for } k = 3, \ldots, N \tag{3.41}$$

It turns out that the unique solution for the $N-2$ equations is given by [2]:

$$\begin{aligned} ln(D_i) = &- (-0.5i+1)(i-1)ln(D_0) \\ &- i(i-2)ln(D_1) + 0.5i(i-1)ln(D_2) \quad i = 3, \ldots, N \end{aligned} \tag{3.42}$$

These equations can then be inserted into Equations 3.37, 3.38 and 3.39 and solved with a non-linear solver. Here, it was done by using the fsolve(...) function of the open-source library SciPy for Python which is using a Jacobian-based gradient descent method.

3.6 Binomial-Like Distribution

The binomial-like distribution assigns the probability $P(k)$ of all possible patterns with k spikes as

$$P(k) = \eta\delta_{0,k} + (1-\eta) \cdot B_{N,\epsilon}(k) \tag{3.43}$$

where η is the percentage of bins where no spikes is inserted, N is the number of stimulated neurons and ϵ is the copying probability in this part $(1-\eta)$ of the bins where spikes are inserted. $\delta_{0,k}$ denotes the Kronecker-Delta and is 1 if and only if $k = 0$. Thus, sampling from this binomial distribution can be understood as two-step process. First, a random number between (0,1) is generated and if this number is less than η, then no spikes are inserted. Otherwise, a random integer number from a binomial distribution with parameters N and ϵ is drawn and this number of spikes is randomly placed in the input neurons.

The choice of taking this binomial-like distribution is inspired by the Multiple Interaction Processes (MIP) which was studied in the past [14]. This distribution has a low variance and low entropy which is significantly different from the other distributions.

For a fixed number of stimulated neurons N, there are two free parameters here: ϵ and η. Those two parameters are chosen such that this distribution has a prescribed mean firing rate μ and pairwise correlation coefficient c. This fit was done by using the fsolve(...) function of the open-source library SciPy for Python.

3.7 Comparison of the Input Distributions

We now derived three different input distributions: One with maximal entropy, one with zero higher-order correlations (zero HoC) and one binomial-like distribution. To compare them, we can plot the assigned pattern probability on a normal scale and a log-scale in figure 3.5 for $N = 50, \mu = 0.1$ and $c = 0.02$. We can observe that they behave relatively similar for a small number of synchronous spikes ($k < 15$) with the main difference that the binomial distribution assigns a higher probability to the pattern with zero spikes. For higher k ($k > 15$), the probability distributions diverge. The maximum entropy distribution remains relatively constant which is expected because a system has maximal entropy for a uniform distribution. The other two distribution drop rapidly with the binomial distribution dropping even faster.

Another way of comparing the three distributions is in terms of entropy. The maximum entropy distribution obviously has the highest entropy, the zero HoC distribution has a medium entropy and the binomial distribution has a very low entropy due to less variance in the distribution. When we compare the distributions in terms of the third-order cumulants, we find that the maximum entropy distribution has a positive cumulant whereas the binomial distribution has a negative cumulant and the zero HoC has a zero cumulant. In a way, the input distributions are chosen to have completely different properties to maximize the differences in the evoked activity.

3.8 Generating Data from Pattern Distributions

Generating data from the pattern distributions obtained in the previous chapters is now straight-forward.

1. First, we have to decide upon on a bin size τ, e.g. $\tau = 20$ms.

2. Then for each bin, we sample from one of the distributions (Zero Higher-Order Correlations, Maximum Entropy or Binomial-Like) shown in figure 3.5. The sampled value corresponds to the number of synchronous spikes k per bin.

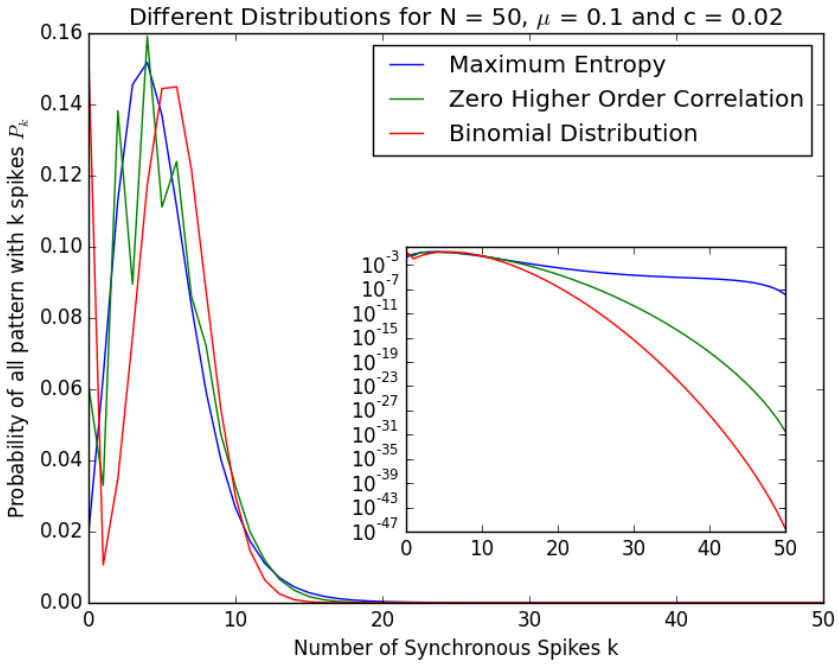

Figure 3.5. Probability of pattern distributions. Inset: Log-Scale

3. We then randomly select k out of the N neurons and insert a spike. The spike timing can either be in the middle of the bin or with any other distribution in the bin, e.g. randomly placed within a bin. For all of the simulations, the second method is chosen.

This gives us an input with the desired firing rates, pairwise correlation coefficient and higher-order statistics. Figure 3.6 shows 3 times 50 Neurons with the input sampled from the three different distributions. Even though, the first two moments are the same, it is possible to see some small differences, e.g. the binomial-like distribution has a higher probability of no spikes at all and the maximum-entropy distribution has a higher probability of a large number of synchronous spikes.

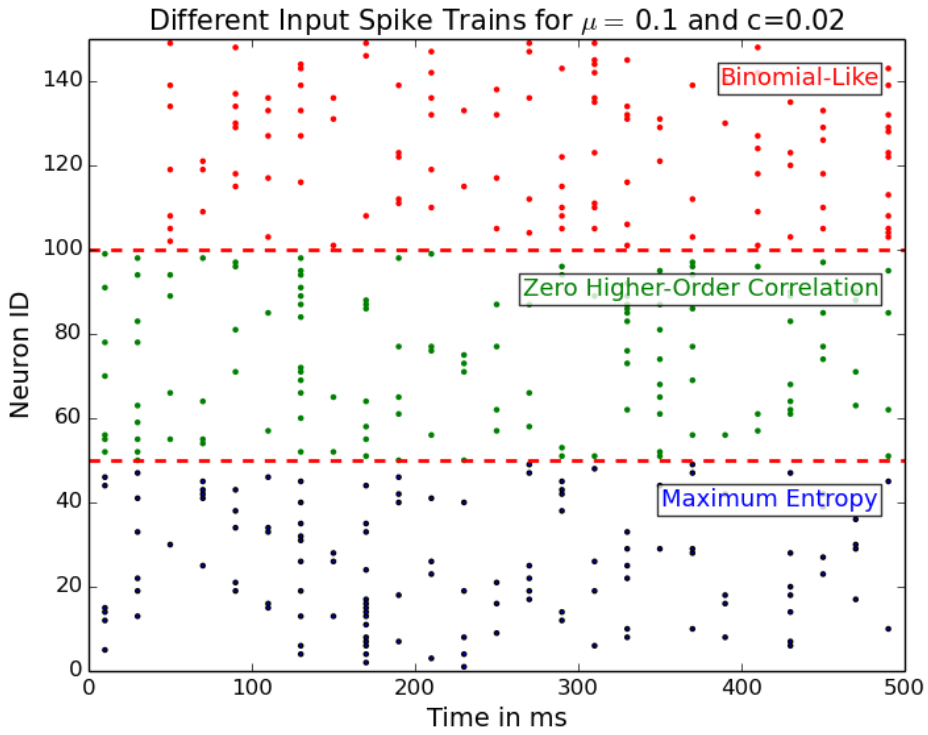

Figure 3.6. Input spike trains with different pattern distributions and bin-centered spikes

Chapter 4

Data Analysis Methods

In order to analyze the simulated data, different spike trains statistics are commonly used. The underlying idea of a spike train is to just look at the spiking times, but not at the sub-threshold dynamics. Let y_i denote the spiking times of the i-th neuron and let $\langle . \rangle$ denote a time-average. The mean firing rate is then given by $\nu_i = \langle y_i \rangle$ for $i = 1, \ldots, N$. Because we assume stationary, firing rates are commonly computed over the whole stimulation length. The variability in firing rates across brain regions, neuron types and tasks is immense, but generally, it is well-established that higher firing rates are associated with a higher level of information processing.

Electrical activity emanating from the brain is sometimes, but not always, displayed in the form of brainwaves which are classified into different frequency bands. Delta waves (1-4 Hz) are the slowest waves which are often observed during dreamless sleep. Theta waves (4–8 Hz) are often associated with REM sleep and the transition from sleep to wakefulness. Alpha waves (8-13 Hz) predominantly originate from the occipital lobe during wakeful relaxation with closed eyes. It is commonly observed that opening the eyes leads to a replacement of alpha waves by beta waves (13-30 Hz), a phenomena called Berger-effect. Beta waves are usually associated with a state of wide wakefulness. Gamma waves (30Hz+), the fastest kind of oscillations, were linked to intense concentration, cognitive processing or meditation.

Besides measuring the firing rates of the neurons, one is often interested in measuring how regularly neurons fire. A commonly used measurement is the coefficient of variation (CV) of the inter-spike interval (ISI). The inter-spike interval (ISI) denotes the distance between two subsequent spikes within one spike train. The coefficient of variation (CV) of the ISI distribution is given by

$$CV_{ISI}^2 = \frac{\sigma_{ISI}^2}{\mu_{ISI}^2} \tag{4.1}$$

where σ_{ISI} denotes the standard deviation of the ISI distribution and μ_{ISI} its mean. A lower CV_{ISI}^2 means that the spike-train is more regular whereas a higher CV_{ISI}^2 indicates a more irregular spike train. If the spike train is a Poissonian spike train,

then $CV_{ISI} = 1$. For $CV_{ISI} < 1$, the spike trains are more regular, slowly becoming periodic. In the extreme case of $CV_{ISI} = 0$, the spikes occur at a certain frequency without any variation. For $CV_{ISI} > 1$, the spike train is very irregular. Commonly observed CV_{ISI} in the visual cortex are in the range of 0.5-1.2 [25].

Additionally to single neuron statistics, one often wants to quantify the dependencies between multiple neurons. For pairs of neurons, the pairwise correlation coefficient between spike trains $y_i(t)$ and $y_j(t)$ was computed with the Pearson correlation coefficient as

$$\rho_{ij} = \frac{Cov(y_i, y_j)}{\sqrt{Cov(y_i, y_i)Cov(y_j, y_j)}} \tag{4.2}$$

where $Cov(y_i, y_j) = \langle (y_i(t) - \nu_i)(y_j(t) - \nu_j) \rangle = \langle y_i(t) y_j(t) \rangle - \nu_i \nu_j$. The time averaging was done with a binsize of 200ms. Again, the observed pairwise correlations in the brain vary based on the region, study and task. The highest correlations were measured in the visual cortex and are around 0.18-0.25 [7]. Very small correlations of only 0.02 were measured in the retina [22] and most other correlations are somewhere in between.

Another statistic of interest is measuring the variability of the responses to the same stimulus across different trials. To that end, the Fano-Factor of the spike counts across trials is computed. It is an indicator for the reliability of the responses. A low Fano-Factor corresponds to neurons which fire with a small variation around their average firing rates, whereas a large Fano-Factor corresponds to neurons which firing rates varies a lot around the average firing rate.

The Fano-Factor is constructed in the following way: (1) The network is stimulated for a certain number of trials. (2) For each trial, the activity of the same neurons is recorded. (3) The recorded activity is binned into time bins of length 200ms, which is called the spike counts σ_i. Note that this spike count can take values above 1 whereas earlier in the maximum-entropy model the value was restricted to 1 or 0. (4) For each neuron and time bin, the mean and variance of the spike counts across trials is computed. (5) The Fano-Factor of the i-th neuron and j-th time bin is then given by

$$FF_i^j = \frac{Var[\sigma_i^j]}{E[\sigma_i^j]}. \tag{4.3}$$

(6) Optional: The Fano-Factor is averaged across neurons and across time bins.

A commonly observed phenomena is the reduction of the Fano-Factor with stimulus onset. This is believed to be linked to a more efficient usage of neural hardware. Values before stimulus onset range from 1.2-2 depending on the brain region and decrease to 0.95-1.2 for the same regions [6].

To guarantee an an efficient and verified implementation of these data analysis methods, the Python package NeuroTools was used [9].

4.1 Tukey's test

To evaluate the significance of the simulation results, Tukey's test was applied in chapter 5. In Tukey's test, the mean value of every method is compared with every other method. The idea is to simultaneously test the differences of all pairwise means $\mu_i - \mu_j$ and identifies those where the difference is exceeding the expected standard error.

The test is essentially a T-test which is corrected for the fact that multiple comparisons are made. The test statistic is given by:

$$q_s = \frac{\mu_A - \mu_B}{SE} \tag{4.4}$$

where μ_A is the larger of the two means being compared, μ_B is the smaller of the two means being compared, and SE is the standard error of the data. The value of q_s can then be compared to a q value from the studentized range distribution to determine whether the differences are significant or not. The studentized range distribution is a generalisation of the Student's t distribution. Tukey's test has the advantage of providing confidence intervals as well.

To apply Tukey's test, the three conditions have to be satisfied:

1. The observations being tested are independent within and among the groups.
2. The groups are normally distributed.
3. There is equal within-group variance across the groups (homogeneity of variance).

Chapter 5

Results

In this chapter, the results will be presented. The first part of the results will show the effect of different between correlations on the network dynamics for different network types. The second part will then show the effects of different higher-order correlations for fixed pairwise correlation coefficients.

5.1 Varying the Between Correlations

In this part, input distributions with different between correlation are generated. The input is always created with a Compound Poisson Process with a binomial amplitude distribution as described in section 3.2.

5.1.1 Neocortex-type of Network

The neocortex is a part of the mammalian brain comprising both the motor and visual cortex. Networks within the neocortex typically have recurrently and mutually connected excitatory and inhibitory neurons with distance dependent connectivity. See again figure 2.3**A** for an illustration of this network connectivity. In the simulations, the network is driven by external independent Poisson input and after the stimulus onset, one part of the network is additionally driven by the stimulus. All network parameters can be found in the appendix.

First, we want to verify that the choice of network connectivity and parameters creates dynamics that are typically observed during the ongoing activity in the neocortex. The network was simulated with 50 trials á 10 seconds. The spiking activity is characterized by low firing rates ($v = 6.63 \pm 0.261$Hz, variance across trials), irregular inter-spike intervals ($CV = 1.04 \pm 0.011$, variance across trials) [25], high local pairwise correlation coefficient in 200 neighbouring neurons ($\rho_{local} = 0.10 \pm 0.013$, time bin 200ms) and low global pairwise correlation coefficients ($\rho_{global} = 0.043 \pm 0.007$, time bin 200ms) [7] and an asynchronous global activity characterized by no regular fluctuations in the histogram. This state can be characterized as asynchronous irregular (AI) where the network operates in the

fluctuation-driven regime, i.e., when mean inputs are subthreshold and spiking occurs as a result of fluctuations (see [4] for an overview of different activity states). Figure 5.1 and figure 5.2 show a typical spike raster plot for 500ms before the stimulus and 500ms after stimulus onset for different between correlations.

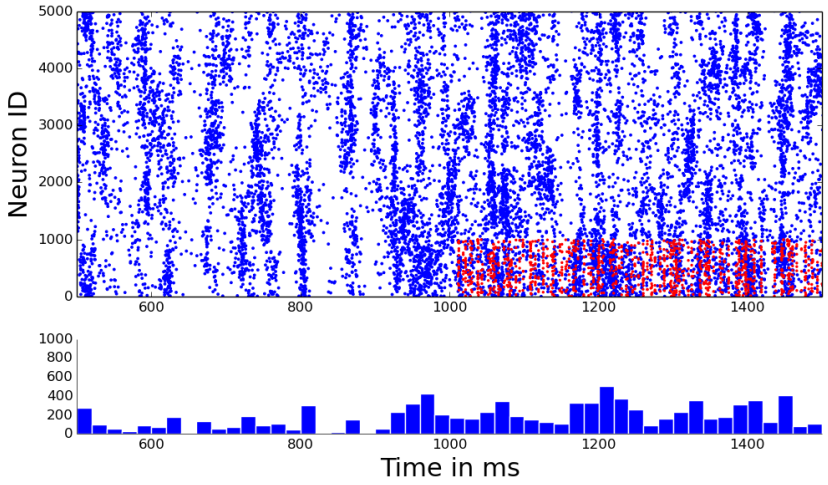

Figure 5.1. Network Activity. Top: Spike raster plot. Each blue dot represents a spike from one neuron at a given time. The red dots show the feedforward input spikes in a local part of the network (1000neurons) with a rate of 5Hz per neuron. Every third neuron is plotted. **Bottom:** Spike activity histogram with binsize 20ms.

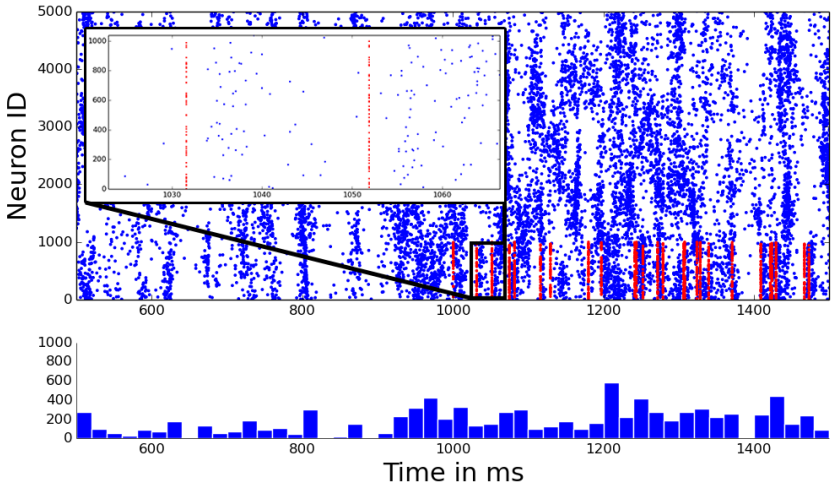

Figure 5.2. Plots as before with higher between correlations in the input. **Inset** shows local network response to a set of inputs.

A straightforward question to ask is how the evoked dynamics change when keeping the total number of incoming spikes constant, but changing the between correlations in the input (see again figure 5.1 and figure 5.2 for an illustration of these different inputs). To study this question, we fix the total number of incoming spikes at 5Hz per neuron. The within correlations which modifies the strength of the input spikes is chosen in such a way that an incoming spike has a high probability to elicit a spike (see inset of figure 5.2). The between correlation were varied in $\{0.01, 0.05, 0.1, 0.15, 0.2\}$ representing a range from very low to relatively high correlations. The network was simulated for 50 times 10 seconds and different statistics were computed (figure 5.3). Global statistics always refer to the whole network whereas local statistics refer to the stimulated part of the network.

First, one can observe typical characteristics of the evoked response, i.e. increased firing rates [6] and an increase or decrease in noise correlations [21]. The Fano Factor across trials is increasing which does not match with current findings from experimental data [17]. This is mainly due to the fact the Fano Factor (FF) before stimulus is on a very low Poissonian level of around 1.06 and the additional Poissonian input cannot further reduce this FF. In fact, the opposite is the case. The stimulus is increasing the variance in one part of the system which actually leads to a small increase in FF.

Comparing the evoked activities, the general trend is that higher between correlations lead to (a) lower global and local firing rates, (b) higher global and local pairwise correlation coefficients and (c) an increased variability in the peristimulus histogram (PSTH) despite lower firing rates. This is the case despite the fact that all inputs have the same frequencies. While the first finding is rather unexpected, the second and third findings are somewhat expected, because higher between correlation naturally lead to higher pairwise correlations and also impose a higher variability over time. The other parameters, the coefficient of variation (CV) of the inter-spike interval (ISI) and Fano Factor (FF) across trials, were not significantly different for different between correlations.

Most interestingly is the first finding, namely that temporally distributed input is more efficient than highly synchronous input. The reason is probably linked to the idea of "spike-wasting" [14]. Because the network is relatively balanced, only few input spikes are necessary to elicit a local activity. But when too much synchronous input arrives, then they cancel out due to the excitatory/inhibitory balance and do not have any further effect on the network behaviour. Thus, the input spikes are "wasted" which reduces the firing rate for highly synchronous input patterns.

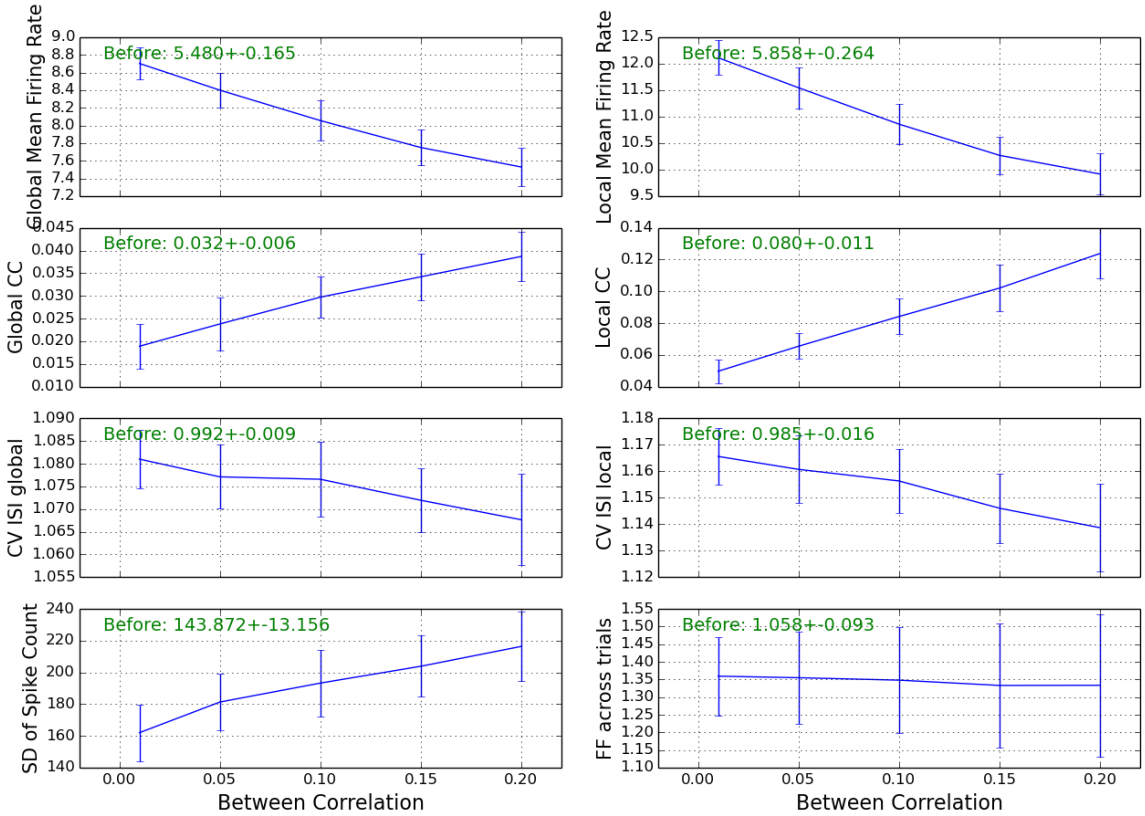

Figure 5.3. Influence of between correlations on the network dynamics quantified by various output statistics. Plots were generated from 50 Simulations a 10 seconds. "Before" denotes the mean and standard deviation across trials before stimulus. Confidence intervalls show 1σ interval across trials. The following abbreviations are used: CC=Pearson Correlation Coefficient, 200ms bins, CV ISI=Coefficient of Variation of the Inter-Spike Interval, SD=Standard Deviation of spike count in 20ms bins, FF=Fano Factor, 200ms bins. See chapter 4 for an explanation of the statistics.

5.1.2 CA1-type of Network

Not all parts of the mammalian brain have recurrently and mutually connected excitatory and inhibitory neurons. For instance, the CA1 area in hippocampus is lacking recurrent excitatory connections. We also modelled this network as shown in figure 2.3**B**. A list of all parameters is shown in the appendix. Note that due to the absence of excitatory to excitatory connections, the connectivity is more sparse than in the neocortex type of network. Again, we simulated the network for 50 times 10 seconds. The results are shown in figure 5.4.

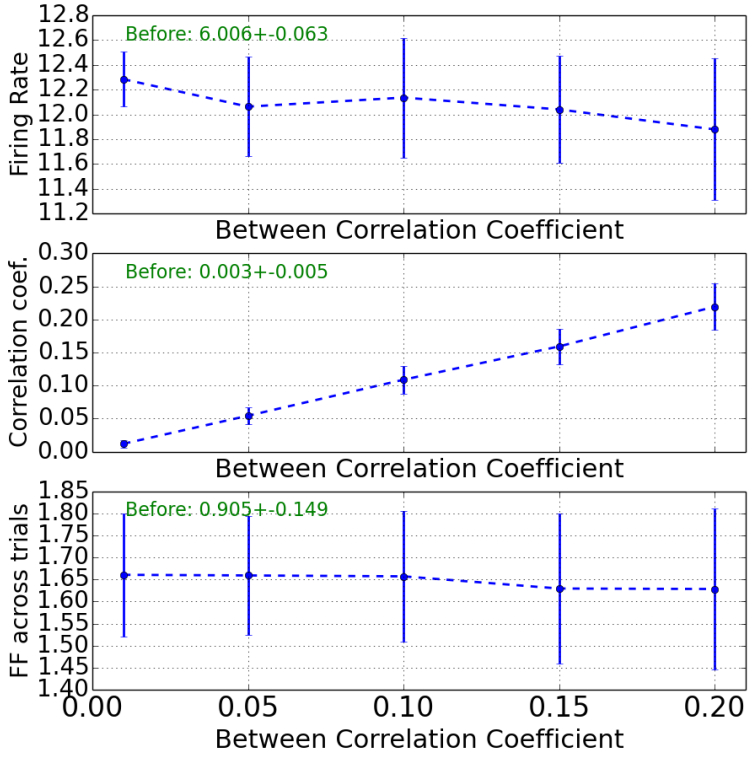

Figure 5.4. Influence of between correlations for a CA1-type of network.

One can see that the firing rate does not vary much with the input correlations. This finding suggests that indeed the balance between excitation and inhibition is responsible for the reduced effectiveness of highly correlated input. On the other hand, the pairwise correlations are almost linearly depending on the input correlations. The Fano Factor across trials and the CV of the ISI (not shown) do not vary significantly for different between correlations.

5.1.3 Striatum-type of Network

The basal ganglia is a well-connected part of the brain which is associated with a variety of functions including action selection and reinforcement learning. The striatum, a network within the basal ganglia, has three very interesting properties [31]: (1) It receives strong input from the cerebral cortex. The input is special in the way that a very large number of neurons in the cortex map to a small number of neurons in the striatum. It is estimated that spiny neurons each receive about 10,000 synaptic contacts from excitatory axons. (2) The pairwise correlations in striatum are very small and (3) it is lacking excitatory neurons making it a purely inhibitory network.

This large number of incoming synapses suggests that much of the synaptic input is shared. In this computational study, we now want to examine the effect of the amount of the shared inputs, especially on the output correlation coefficient.

The network in the ongoing activity is tuned to exhibit asynchronous irregular (AI) dynamics characterized by medium firing rates ($\nu = 5.9$Hz), irregular activity ($CV = 0.955$, $FF = 0.938$) and almost no correlations ($\rho = 0.00$). The parameters can be found in the appendix. See figure 5.5 for a raster plot of the activity.

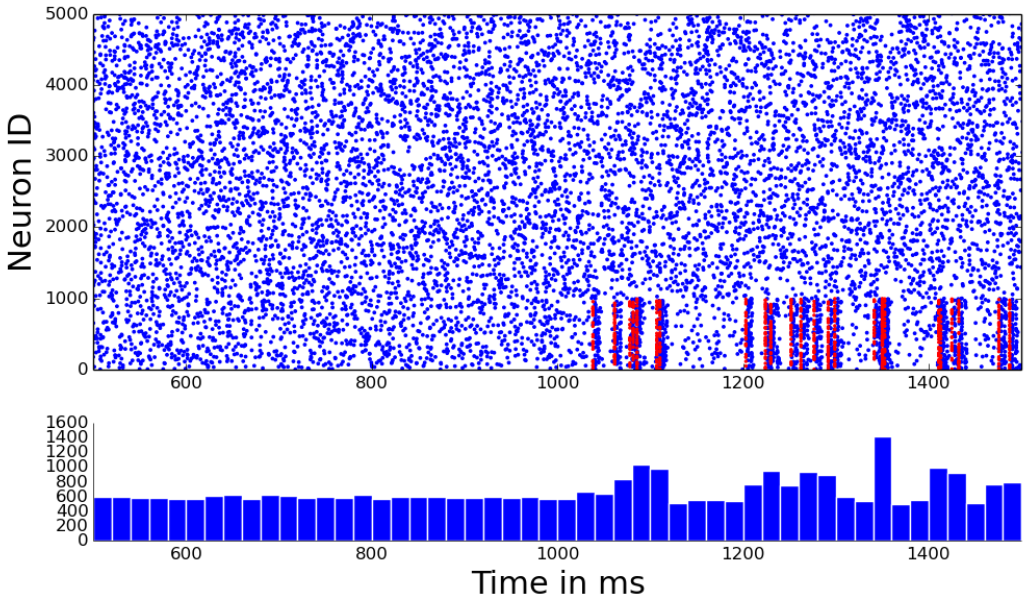

Figure 5.5. Raster plot for activity in striatum-type of network

Recordings from the striatum typically show a low level of pairwise correlations. How is this possible despite the large number of inputs? The answer lies in the spatial arrangement of the receptor fields and the mutual inhibition of the neurons. Even though the number of synaptic inputs is large, each of the neurons shares

only 2-3% of its synaptic input [31]. The reason is an extremely sparse sampling in the dendritic fields, i.e. the receptor fields only overlap to a very small degree. If we look at the network dynamics in figure 5.6, we can observe that the firing rates behave similar to the CA1-type of network. The pairwise correlations increase very slowly with the input between correlation. This is the effect of the mutual inhibition where the activity of one neuron is suppressing the activity of the other surrounding neurons. This time, there is a small effect on CV, ISI and FF. Higher between correlations drive the network more towards Poissonian dynamics with $CV = 1$ and $FF = 1$.

In summary, each neuron receives highly correlated input from many neurons (large within correlations) which is relatively independent of each other (low between correlations). This leads to a network dynamic which is characterized by a relatively low pairwise correlation coefficient. This case study emphasizes the difference between correlations in the divergent and convergent connections.

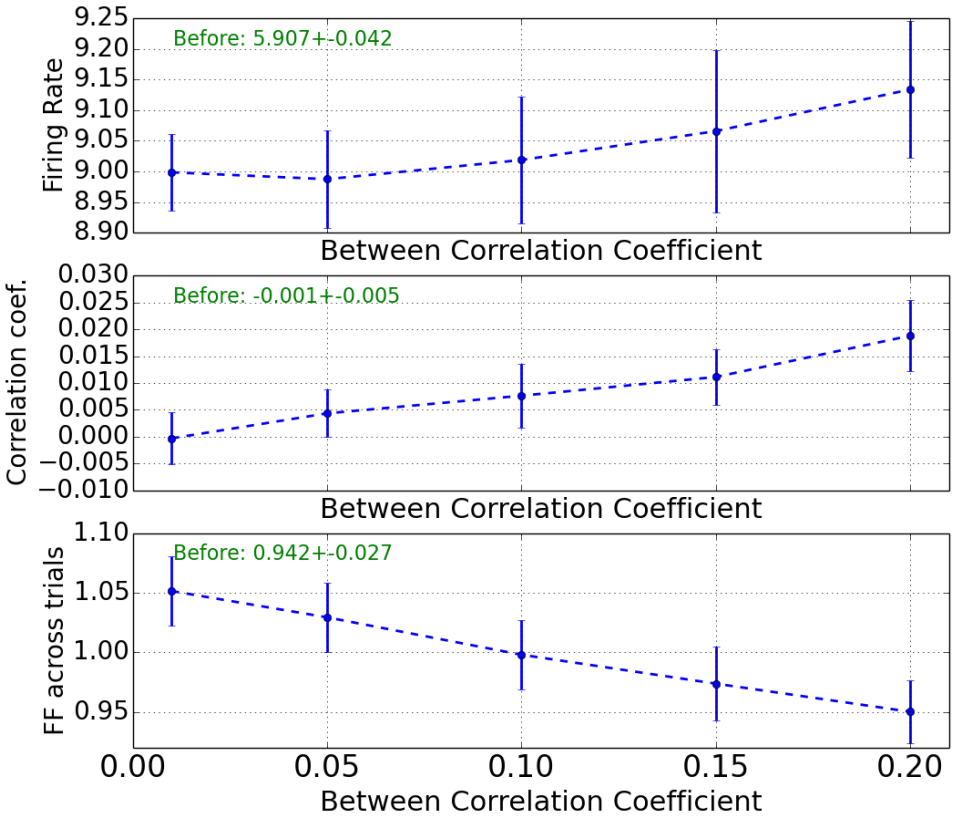

Figure 5.6. Output statistics for striatum-type of network.

5.2 Varying Higher-Order Correlation for fixed Between Correlations

In the previous subsection, we have shown how different between correlations can lead to different network activities. They especially affect firing rates and pairwise correlations depending on the network architecture. Given a fixed pairwise between correlation, there are several choices for the higher-order correlation structure. The next step is to explore the effect of these higher-order correlation structures. To that end, the input was generated according to a Compound Poisson Process with the following three different between distributions: (1) Geometric Distribution, (2) Log-Series Distribution and (3) Binomial-Like Distribution as explained in section 3.2. Each of the distributions had the same between correlation of $\rho_b = 0.15$.

The first simulations were run on the neocortical network model with the same parameters as before. Significance of the different statistics was tested with a Tukey's test which compares the pairwise means of the output statistics obtained by using one of three input distributions. It identifies any difference between two means that is greater than the expected standard error. Variances of all populations were very similar, they were approximative normally distributed and independent of each other. Hence, they satisfy the assumptions for this test. Figure and table 5.7 show a graphical comparison of the output statistics and the differences in means and their significance.

It can be seen that significant differences in mean exist, but they are still very small. The largest differences occur for local firing rates and pairwise correlations coefficients. For the firing rates, they are about 1-5% and partially significant. For the pairwise correlation coefficient, the differences are all significant, about 10-20% in relative difference, but only about 0.01-0.02 in absolute numbers. These findings suggest that the influence of the higher-order correlation structure in the between correlations is very limited even though the between correlation was chosen to be quite high (0.15) and the three input distributions are significantly different from each other (see figure 3.2). Now the question arises whether these findings are specific to this combination of network architecture, neural parameters and input distributions or whether they hold in a more general context. To investigate this question, we followed the following four approaches:

1. Study different network architectures
2. Vary the frequency of the input
3. Decrease the membrane time constant to make the neurons more sensitive to the exact timing of the inputs
4. Use the bin-wise input to directly control the higher-order correlations

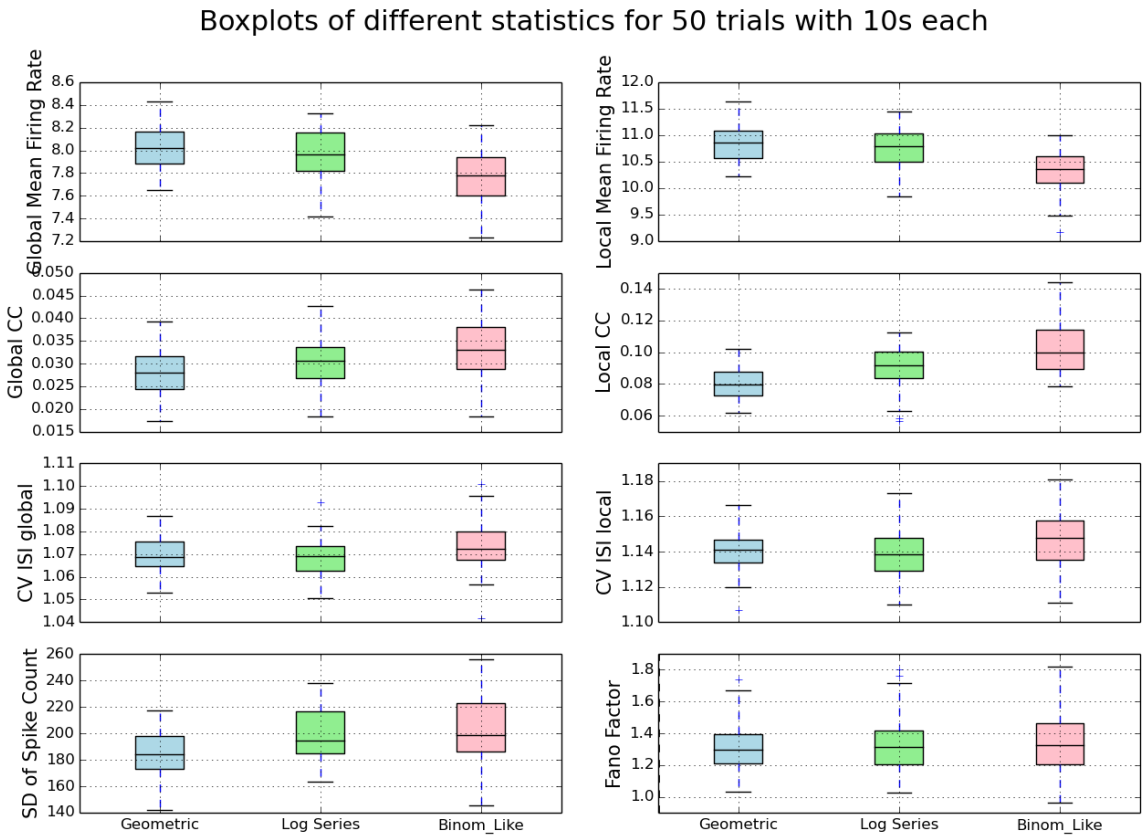

Firing Rates

group1	group2	meandiff	significant
Binomial	Geometric	0.41 (3.83%)	Yes
Binomial	Log Series	0.53 (4.84%)	Yes
Geometric	Log Series	0.11 (1.05%)	No

Pairwise Correlation Coefficients

group1	group2	meandiff	significant
Binomial	Geometric	0.012 (11.45%)	Yes
Binomial	Log Series	0.022 (21.14%)	Yes
Geometric	Log Series	0.010 (10.94%)	Yes

Figure and table 5.7. Top: Boxplots for different input distributions and statistics. Tukey's boxplot is used where whiskers show the lowest datum still within 1.5 interquartile range (IQR) of the lower quartile, and the highest datum still within 1.5 IQR of the upper quartile. **Bottom:** Table showing the absolut and relative differences in mean, and the signifcance of Tukey's test.

5.2.1 Different Network Architectures

To investigate whether higher-order correlations are more important on other network types, we simulated a CA1-type of network and a Striatum-type of network with the same input as before. Here, we focus on the firing rates and pairwise correlation coefficients of the output.

For the CA1-type of network, we find that none of the differences are significant as shown in figure 5.8. The same finding holds for a striatum-type of network as presented in figure 5.9. These findings suggest that excitatory to excitatory connection are necessary to elicit any significant difference in the response to higher-order correlations. Hence, the structure of the network appears to influence the sensitivity of a network to the input higher-order correlation structure.

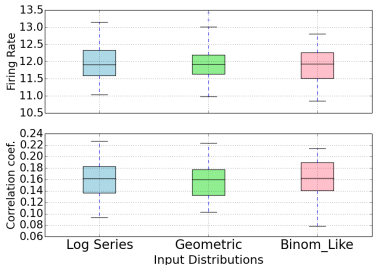

Local firing rates:

group1	group2	meandiff	significant
Binomial	Geometric	0.095 (0.79%)	No
Binomial	Log Series	0.103 (0.86%)	No
Geometric	Log Series	0.009 (0.07%)	No

Local pairwise correlation coefficient:

group1	group2	meandiff	significant
Binomial	Geometric	0.005 (3.17%)	No
Binomial	Log Series	0.002 (1.45%)	No
Geometric	Log Series	0.003 (1.75%)	No

Figure 5.8. Comparison of firing rates and pairwise correlation coefficient for a CA1-type of network.

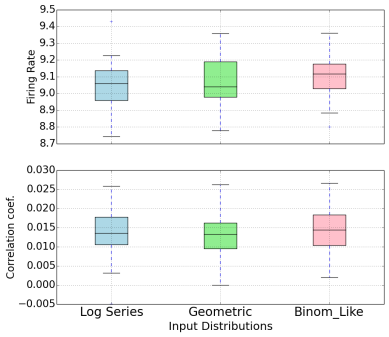

Local firing rates:

group1	group2	meandiff	significant
Binomial	Geometric	0.029 (0.32%)	No
Binomial	Log Series	0.046 (0.50%)	No
Geometric	Log Series	0.016 (0.18%)	No

Local pairwise correlation coefficient:

group1	group2	meandiff	significant
Binomial	Geometric	0.0015 (10.23%)	No
Binomial	Log Series	0.0012 (8.14%)	No
Geometric	Log Series	0.0003 (2.27%)	No

Figure 5.9. Comparison of firing rates and pairwise correlation coefficient for a striatum-type of network.

From now on, all simulations well be done on the neocortex-type of network, because this appears to be the network model where the higher-order correlations matter the most.

5.2.2 Varying the Input Frequency

Another variation to investigate is the frequency of the input. So far, a rate of 5Hz was used in the neocortical-network model. One could suspect that if we increase the importance of the feed-forward input in relation to the ongoing activity, then we can elicit larger differences. Therefore, we increased the input frequency to 15Hz. The network is now much more input-driven. Again, figure 5.10 shows the output firing rates and pairwise correlation coefficients.

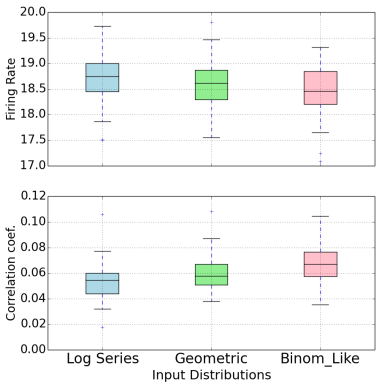

Local firing rates:

group1	group2	meandiff	significant
Binomial	Geometric	0.1165 (0.63%)	No
Binomial	Log Series	0.2529 (1.35%)	Yes
Geometric	Log Series	0.1364 (0.73%)	No

Local pairwise correlation coefficient:

group1	group2	meandiff	significant
Binomial	Geometric	0.0087 (12.87%)	Yes
Binomial	Log Series	0.0147 (21.72%)	Yes
Geometric	Log Series	0.006 (10.15%)	No

Figure 5.10. Comparison of firing rates and pairwise correlation coefficient for increased input frequency.

The relative differences in firing rate decrease while the absolute difference increases. This is probably due to the fact that the network is more constantly driven by the input and the exact timing of the input is less important. The relative differences in pairwise correlation are similar to before. Another idea was to decrease the input frequency to increase the spatial distribution of the input. Figure 5.11 shows that this slightly increases the relative differences in firing rates. However, further reducing the input frequency will put the network into a state where it is not driven by the input any more and no differences are visible.

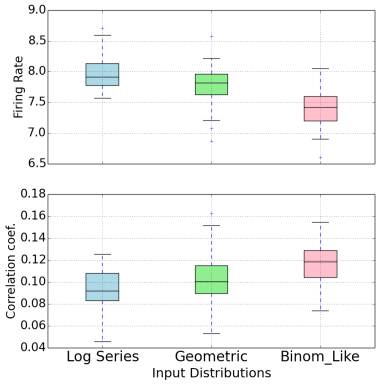

Local firing rates:

group1	group2	meandiff	significant
Binomial	Geometric	0.367 (4.72%)	Yes
Binomial	Log Series	0.583 (7.29%)	Yes
Geometric	Log Series	0.215 (2.70%)	Yes

Local pairwise correlation coefficient:

group1	group2	meandiff	significant
Binomial	Geometric	0.015 (12.86%)	Yes
Binomial	Log Series	0.024 (20.45%)	Yes
Geometric	Log Series	0.009 (8.71%)	No

Figure 5.11. Comparison of firing rates and pairwise correlation coefficient for decreased input frequency.

5.2.3 Decreased Membrane Time Constant

Next, we hypothesised that the membrane time constant of the neurons can affect the sensibility to higher-order correlations. The membrane time constant as defined in section 2.1.1 is influencing the time-scale of the neurons. A neuron with a small time constant is integrating the input faster than a neuron with a larger time scale. We hypothesised that reducing the time constant from 10ms to 5ms makes the neuron more sensitive to the exact timing of the spikes and therefore, more sensitive to higher-order correlations. To test this, the neocortical-type of network was simulated with an input frequency of 5Hz and a membrane time constant of 5ms. The time constant is still in a physiological measured range [12]. The other parameters such as synaptic strengths had to be slightly adjusted to have the similar kind of ongoing activity as before. All parameters are given in the appendix. Figure 5.12 shows the results.

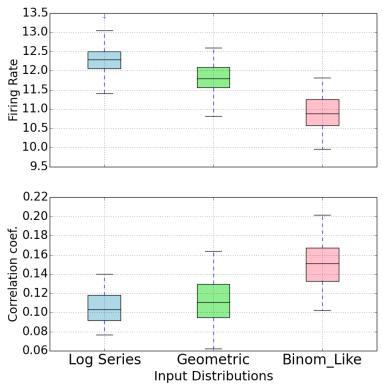

Local firing rates:

group1	group2	meandiff	significant
Binomial	Geometric	0.912 (7.71%)	Yes
Binomial	Log Series	1.377 (11.20%))	Yes
Geometric	Log Series	0.465 (3.78%)	Yes

Local pairwise correlation coefficient:

group1	group2	meandiff	significant
Binomial	Geometric	0.036 (23.85%)	Yes
Binomial	Log Series	0.045 (29.96%)	Yes
Geometric	Log Series	0.009 (8.03%)	No

Figure 5.12. Comparison of firing rates and pairwise correlation coefficient for decreased membrane time constant.

One can see that the differences significantly increased confirming the hypothesis from above. The differences in firing rate can exceed 10% now and the differences in pairwise correlations goes up to 30%. To further investigate the matter, we looked at the length of the sustained activity, i.e. the length how long the activity persist after the input has stopped. Figure 5.13 shows that the length of the sustained activity is around 10ms in both scenarios. So the question remains why neurons with shorter time scales are more sensitive to higher-order correlations than neurons with faster time scales. An intuitive answer is that neurons with longer time scales are blurring and averaging the input over a broader interval than neurons with short time scales. Hence, neurons with shorter time scales are more sensitive to the exact timing of the input.

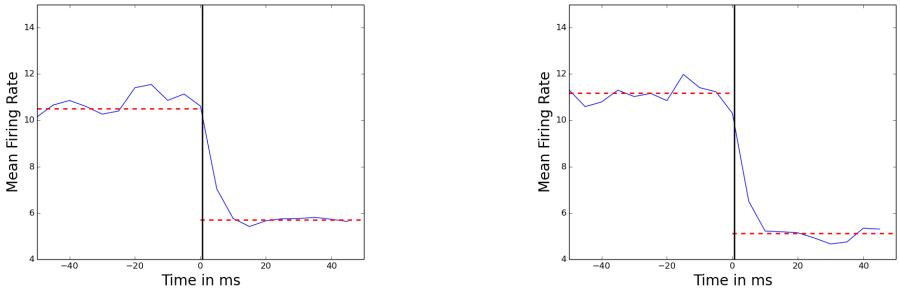

Figure 5.13. Length of sustained activity. Mean firing rate was measured with respect to 5ms bins and averaged over 500 trials. Vertical black bar indicates the end of the stimulus. Red dashed line indicates the average during and after stimulus. **Left:** Time constant equals 10ms. **Right:** Time constant equals 5ms.

5.2.4 Bin-wise Input in Mean-driven Dynamics

So far, we simulated input with relatively high pairwise correlation coefficients of 0.15. Now, we want to simulate a mean-driven network characterized by a regular activity with weak pairwise correlations of 0.02 which can be found in the ganglion cells in the retina [22]. The connectivity is the same as in the neocortex with recurrent and mutually connected excitatory and inhibitory cells. The number of cells is now reduced from 5000 to 250, because of the limitations of the bin-wise input as explained in section 3.4.5. However, this number is still sufficient to avoid finite-size effects. Instead of the Compound Poisson Process, we used the three bin-wise input distributions (Maximum Entropy (Max Ent), Zero Higher-Order Correlations (Zero HoC), Binomial-Like) as derived in chapter 3 to directly control the higher-order cumulants. The differences in the output are very small and not significant as shown in figure 5.14. The reason is probably the small pairwise correlation coefficient and weak synaptic strength in the mean-driven regime.

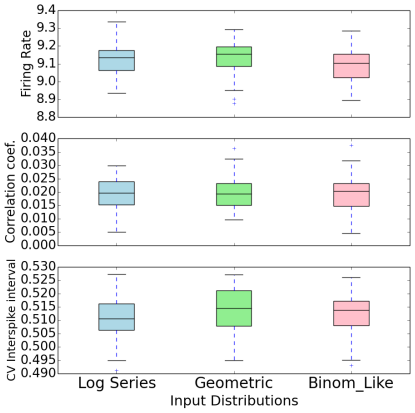

Local firing rates:

group1	group2	meandiff	significant
Binomial	Max Ent	0.031 (0.33%)	No
Binomial	Zero HoC	0.025 (0.27%)	No
Max Ent	Zero HoC	0.006 (0.06%)	No

Local pairwise correlation coefficient:

group1	group2	meandiff	significant
Binomial	Max Ent	0.0001 (0.52%)	No
Binomial	Zero HoC	0.0005 (2.51%)	No
Max Ent	Zero HoC	0.0004 (2.00%)	No

Figure 5.14. Output statistics for the mean-driven regime with bin-wise input.

Chapter 6

Discussion

This work examined the effect of pairwise and higher-order correlations in the feed-forward input to neural networks. It was shown that it is crucial to distinguish between correlations in the convergent connections and correlations in the divergent connections. Correlations in the convergent connections directly modulate the efficiency of the input leading to a significant effect on the evoked dynamics [5]. On the other hand, correlations in the divergent connections only work through synaptic connections and have a less pronounced effect on the network dynamics. It was shown that they mainly modulate the output pairwise correlations coefficient and that they also have a small effect on the output firing rates depending on the network type.

The second finding was that distributions with the same individual firing rate and pairwise correlation coefficient, but different higher-order correlations show a very similar response. In CA1-type and striatum-type of networks, the differences were not even significant which suggests that excitatory to excitatory connections are necessary to induce different responses to different higher-order correlation structures. In a neocortial-type of network, the responses were significant, but still relatively small. We found that the differences become larger for a small input frequency and a reduction of the membrane time constant.

Overall, these findings lead to the hypothesis that higher-order correlations carry a limited amount of information as they only have a small effect on the evoked dynamics. These findings could significantly simplify the analysis of neural data, because it would mean that it is only necessary to measure firing rates and pairwise correlations of the divergence connections to approximate the network's activity. Higher-order correlation in the convergent connections can relatively easy be measured by looking at single neurons dynamics over time and reconstructing the strength of the input. If the result holds, than the notoriously hard task to measure higher-order cumulants would not be necessary. These findings also match with the application of Maximum-Entropy Models which could explain about 90% of the higher-order correlational structure by just fitting a maximum entropy model which replicates the given individual and pairwise firing rates [22, 28]. However, the find-

ing is still surprising, because it is known that the higher-order correlation structure in the convergent connections can have a severe effect on the evoked dynamics [5].

Of course, one has to be very careful with this hypothesis, because only a few cases and modulations were tested in this work. One big problem with large-scale neural network simulation is always the freedom in the choice of parameters. Physiological measurements give us a range for the parameters, but these ranges can be very large. We tried to encounter this problem by choosing the parameters in such a way that they are both within the physiological range and also create an activity which is commonly observed in in-vivo measurements. But even with these restrictions, the range of possible parameters is still very large. An even more throughout testing with different parameters might be necessary to confirm this result.

Future work could go also towards a framework which is comprising both within and between correlations in order to explain evoked dynamics. Instead of isolating the effect of those two correlations, one could aim towards a model which combines the effect of both correlations.

Bibliography

[1] Arieli, A. et al. “Dynamics of Ongoing Activity: Explanation of the Large Variability in Evoked Cortical Responses”. In: *Science* 273.5283 (Sept. 1996), pp. 1868–1871.

[2] Bohté, Sander M, Spekreijse, Henk, and Roelfsema, Pieter R. “The effects of pair-wise and higher-order correlations on the firing rate of a postsynaptic neuron”. In: *Neural Computation* 12.1 (2000), pp. 153–179.

[3] Brette, Romain. “Generation of correlated spike trains”. In: *Neural computation* 21.1 (2009), pp. 188–215.

[4] Brunel, N. “Dynamics of sparsely connected networks of excitatory and inhibitory spiking neurons.” In: *J Comput Neurosci* 8 (2000), pp. 183–208.

[5] Bujan, Alejandro F, Aertsen, Ad, and Kumar, Arvind. “Role of Input Correlations in Shaping the Variability and Noise Correlations of Evoked Activity in the Neocortex”. In: *The Journal of Neuroscience* 35.22 (2015), pp. 8611–8625.

[6] Churchland, Mark M. et al. “Stimulus onset quenches neural variability: a widespread cortical phenomenon.” In: *Nature neuroscience* 13.3 (Mar. 2010), pp. 369–378.

[7] Cohen, Marlene R and Kohn, Adam. “Measuring and interpreting neuronal correlations”. In: *Nature neuroscience* 14.7 (2011), pp. 811–819.

[8] Commons, Wikimedia. *Action Potential*.
Image: `Action_potential.svg. From the article "http://en.wikipedia.org/wiki/Action_potential"`.

[9] Daniel Bruederle, Andrew D. and Yger, Pierre. *NeuroTools*. June 2011.

[10] Eppler, Jochen Martin et al. “PyNEST: a convenient interface to the NEST simulator”. In: *Frontiers in neuroinformatics* 2 (2008).

[11] Gewaltig, Marc-Oliver and Diesmann, Markus. “NEST (NEural Simulation Tool)”. In: *Scholarpedia* 2.4 (2007), p. 1430.

[12] Goto, Yukiori and O’Donnell, Patricio. “Delayed mesolimbic system alteration in a developmental animal model of schizophrenia”. In: *The Journal of neuroscience* 22.20 (2002), pp. 9070–9077.

[13] Hennequin, Guillaume, Vogels, Tim P, and Gerstner, Wulfram. "Optimal control of transient dynamics in balanced networks supports generation of complex movements". In: *Neuron* 82.6 (2014), pp. 1394–1406.

[14] Kuhn, Alexandre, Aertsen, Ad, and Rotter, Stefan. "Higher-order statistics of input ensembles and the response of simple model neurons". In: *Neural Computation* 15.1 (2003), pp. 67–101.

[15] Kumar, Arvind et al. "Challenges of understanding brain function by selective modulation of neuronal subpopulations." In: *Trends in neurosciences* 36.10 (Oct. 2013), pp. 579–586.

[16] Litwin-Kumar, Ashok and Doiron, Brent. "Slow dynamics and high variability in balanced cortical networks with clustered connections". In: *Nature neuroscience* 15.11 (2012), pp. 1498–1505.

[17] Oram, Mike W. "Visual stimulation decorrelates neuronal activity." In: *Journal of neurophysiology* 105.2 (Feb. 2011), pp. 942–957.

[18] Renart, Alfonso et al. "The asynchronous state in cortical circuits". In: *science* 327.5965 (2010), pp. 587–590.

[19] Rocha, Jaime de la et al. "Correlation between neural spike trains increases with firing rate". In: *Nature* 448.7155 (Aug. 2007), pp. 802–806.

[20] Rotter, Stefan and Diesmann, Markus. "Exact digital simulation of time-invariant linear systems with applications to neuronal modeling". In: *Biological cybernetics* 81.5-6 (1999), pp. 381–402.

[21] Ruff, Douglas A. and Cohen, Marlene R. "Attention can either increase or decrease spike count correlations in visual cortex." In: *Nature neuroscience* 17.11 (Nov. 2014), pp. 1591–1597.

[22] Schneidman, Elad et al. "Weak pairwise correlations imply strongly correlated network states in a neural population". In: *Nature* 440.7087 (2006), pp. 1007–1012.

[23] Schultze-Kraft, Matthias et al. "Noise Suppression and Surplus Synchrony by Coincidence Detection". In: *PLoS Comput Biol* 9.4 (Apr. 2013), e1002904+.

[24] Shadlen, Michael N and Newsome, William T. "The variable discharge of cortical neurons: implications for connectivity, computation, and information coding". In: *The Journal of neuroscience* 18.10 (1998), pp. 3870–3896.

[25] Softky, William R and Koch, Christof. "The highly irregular firing of cortical cells is inconsistent with temporal integration of random EPSPs". In: *The Journal of Neuroscience* 13.1 (1993), pp. 334–350.

[26] Staude, Benjamin, Grün, Sonja, and Rotter, Stefan. "Higher-order correlations and cumulants". In: *Analysis of parallel spike trains*. Springer, 2010, pp. 253–280.

[27] Staude, Benjamin, Rotter, Stefan, and Grün, Sonja. “CuBIC: cumulant based inference of higher-order correlations in massively parallel spike trains”. In: *Journal of Computational Neuroscience* 29.1-2 (2010), pp. 327–350.

[28] Tang, Aonan et al. “A maximum entropy model applied to spatial and temporal correlations from cortical networks in vitro”. In: *The Journal of Neuroscience* 28.2 (2008), pp. 505–518.

[29] Watts, Duncan J and Strogatz, Steven H. “Collective dynamics of "small-world" networks”. In: *nature* 393.6684 (1998), pp. 440–442.

[30] White, JG et al. “The structure of the nervous system of the nematode Caenorhabditis elegans: the mind of a worm”. In: *Phil. Trans. R. Soc. Lond* 314 (1986), pp. 1–340.

[31] Wilson, CJ. “Active decorrelation in the basal ganglia”. In: *Neuroscience* 250 (2013), pp. 467–482.

[32] Yeh, Fang-Chin et al. “Maximum entropy approaches to living neural networks”. In: *Entropy* 12.1 (2010), pp. 89–106.

Appendix A

Parameters

Here, the simulation parameters are listed. All other parameters are not varied and listed in table 2.1, table 2.2 and table 2.3.

A.1 Neocortex-type of Network

Symbol	Meaning	Value
J_{exc}	Excitatory synaptic strength	50.0
J_{inh}	Inhibitory synaptic strength	-250.0
ν_{ext}	External Poisson rate	250Hz
ν_{ind}	Poisson rate in the stimulated part of the network	200Hz
J_{ext}	External synaptic strength	100.0
ν_{corr}	Frequency of correlated input	5Hz
J_{corr}	Synaptic strength of the correlated input	2000.0

A.2 CA1-type of Network

Symbol	Meaning	Value
J_{exc}	Excitatory synaptic strength	50.0
J_{inh}	Inhibitory synaptic strength	-250.0
ν_{ext}	External Poisson rate	350Hz
ν_{ind}	Poisson rate in the stimulated part of the network	280Hz
J_{ext}	External synaptic strength	100.0
ν_{corr}	Frequency of correlated input	5Hz
J_{corr}	Synaptic strength of the correlated input	2000.0

A.3 Striatum-type of Network

Symbol	Meaning	Value
J_{exc}	Excitatory synaptic strength	100.0
J_{inh}	Inhibitory synaptic strength	-10.0
ν_{ext}	External Poisson rate	250Hz
ν_{ind}	Poisson rate in the stimulated part of the network	250Hz
J_{ext}	External synaptic strength	200.0
ν_{corr}	Frequency of correlated input	10Hz
J_{corr}	Synaptic strength of the correlated input	1000.0

A.4 Decreased Membrane Time Constant

In this scenario, the membrane time constant τ_m was reduced from 10ms to 5ms. A neocortical network model was used. Due to the reduction of the time constant, the amount of the synaptic input was decreased. Therefore, the synaptic strengths and external input frequency was increased to compensate this effect.

Symbol	Meaning	Value
J_{exc}	Excitatory synaptic strength	52.4
J_{inh}	Inhibitory synaptic strength	-262.0
ν_{ext}	External Poisson rate	360Hz
ν_{ind}	Poisson rate in the stimulated part of the network	288Hz
J_{ext}	External synaptic strength	131.0
ν_{corr}	Frequency of correlated input	5Hz
J_{corr}	Synaptic strength of the correlated input	2620.0

A.5 Bin-wise Input Model in Mean-driven Dynamics

Here, the tonic drive I_E was increased and the synaptic strengths were decreased in order to get mean-driven dynamic.

Symbol	Meaning	Value
J_{exc}	Excitatory synaptic strength	0.4
J_{inh}	Inhibitory synaptic strength	-2.0
ν_{ext}	External Poisson rate	50Hz
ν_{ind}	Poisson rate in the stimulated part of the network	40Hz
J_{ext}	External synaptic strength	2.0
ν_{corr}	Frequency of correlated input	5Hz
J_{corr}	Synaptic strength of the correlated input	20.0
I_E	Tonic synaptic drive	299mA
N	Number of neurons	250

TRITA -MAT-E 2015:56
ISRN -KTH/MAT/E--15/56--SE